SKB

TECHNICAL REPORT 89-18

Radar investigations at the Saltsjötunnel – predictions and validation

Olle Olsson[1] and Kai Palmqvist[2]

[1] Abem AB, Uppsala, Sweden

[2] Bergab, Göteborg

June 1989

SVENSK KÄRNBRÄNSLEHANTERING AB
SWEDISH NUCLEAR FUEL AND WASTE MANAGEMENT CO

BOX 5864 S-102 48 STOCKHOLM
TEL 08-665 28 00 TELEX 13108-SKB

RADAR INVESTIGATIONS AT THE SALTSJÖTUNNEL - PREDICTIONS AND VALIDATION

Olle Olsson[1] and Kai Palmqvist[2]

1 Abem AB, Uppsala, Sweden

2 Bergab, Göteborg

June 1989

ABEM AB
Research and Development
Uppsala
Sweden
Client: SKB

REPORT
ID-no. 89 001
Date: 1989-06-20

RADAR INVESTIGATIONS AT THE SALTSJÖTUNNEL - PREDICTIONS AND VALIDATION

APRIL 1989

OLLE OLSSON

ABEM AB

UPPSALA, SWEDEN

KAI PALMQVIST

BERGAB

GÖTEBORG

ABSTRACT

Borehole radar investigations have been performed in two boreholes drilled along the extent of the Saltjö tunnel in Stockholm, Sweden. Singlehole and crosshole radar measurements were made in the two boreholes which outlined an equilateral triangle. The crosshole data was used to produce tomograms showing the distribution of radar attenuation and slowness (inverse of velocity) in the plane between the boreholes.

There is general agreement between the radar model of the site and the geologic-tectonic model of the site. The radar model of the site contained one major feature which was identified as a fracture zone and the intersection with the tunnel was correctly predicted.

This project has demonstrated the capability of the borehole radar technique to predict the existence, location, and orientation of geologic features (e.g. fracture zones) which can be of significance to the cost and safety when excavating a tunnel. However, further development is needed to be able to use the technique cost effectively for continuous prediction ahead of the tunnel front.

SUMMARY AND CONCLUSIONS

Borehole radar investigations have been performed in two boreholes drilled along the extent of the Saltjö tunnel in Stockholm, Sweden. The objective of the project was to test the investigate the capabilities of the borehole radar technique to predict geological structures prior to tunnel excavation.

Singlehole and crosshole radar measurements were made in the two boreholes which outlined an equilateral triangle. The crosshole data was used to produce tomograms showing the distribution of radar attenuation and slowness (inverse of velocity) in the plane between the boreholes.

The radar model of the site contained one major feature which was identified as a fracture zone. The intersection of the fracture zone with the tunnel was extrapolated from the radar data and found to be in agreement with observations in the tunnel. At the intersection of the fracture zone with the tunnel grouting had to be applied. It has also been found that the radar identifies a number of smaller features which are of practically no significance with respect to tunnel construction. There is general agreement between the radar model of the site and the geologic-tectonic model of the site.

This project has demonstrated the capability of the borehole radar technique to predict the existence, location, and orientation of geologic features (e.g. fracture zones) which can be of significance to the cost and safety when excavating a tunnel. However, further development is needed to be able to use the technique cost effectively for continuous prediction ahead of the tunnel front.

CONTENTS

LIST OF FIGURES

LIST OF TABLES

1 INTRODUCTION

STOSEB, the energy supply company of the Stockholm region, has constructed a heating plant in Solna, where the heat is extracted from purified waste water which is taken from a sewer plant in Bromma. To reduce the load of waste water on Lake Mälaren a tunnel has been built to transfer the cooled waste water to Saltsjön. The tunnel extends from the Solna heating plant to a position in Saltsjön just outside the little island Kastellholmen.

The tunnel has been excavated through full face boring, a technique which is relatively new to Sweden. In connection to the excavation of the tunnel a comprehensive research programme has been conducted which has been coordinated by BeFo.

The project described in this report had the objective to test the predictive capabilites of borehole radar in connection to tunnel excavation. The project has been funded and managed by SKB (Swedish Nuclear Fuel and Waste Management Co.).

Borehole radar is a relatively new investigation technique. Development of a new borehole radar system started in 1983 as a part of the International Stripa Project. The work was performed by a group at the Swedish Geological Co. The work within the Stripa Project resulted in a prototype borehole radar system. It also demonstrated the capability of the radar method to map the location, extent, and character of fracture zones. Probing ranges of up to 100 m were achieved. The large probing range in combination with a resolution on the order of metres makes borehole radar a unique tool for rock characterization. Further development work, funded by SKB, has taken the borehole radar from a prototype to a field system (RAMAC) suited for measurements on a commercial basis.

The RAMAC system has been applied extensively within the SKB research and development programme. Measurements have been performed at the study sites Finnsjön, Ävrö, Klipperås, and Äspö. The investigation range in single hole reflection mode has varied from 40 m at Finnsjön to 120 m at Klipperås depending on the electrical conductivity of the rock.

The current project was set up to test the predictive capabilites of the borehole radar technique. The basic concept was to perform radar measurements in two boreholes along the planned tunnel extension. Based on the radar results a prediction would be made on the geological conditions at the site which later would be compared to results from geological, geophysical, and hydrological investigations in the boreholes and the tunnel.

After completion of the drilling borehole radar investigations were performed and evaluated without access to any other information from the boreholes. The radar results and the radar model of the site was presented in an internal SKB report (Carlsten, Falk, and Olsson, 1987). Then followed mapping of the core, geophysical and hydrological investigations in the boreholes. These results were evaluated and compared to the radar results and a revised model of the site was put forth based on all data available at that time (Andersson, Andersson, Carlsten, Falk, Olsson, and Stråhle, 1987). Hydrogeological mapping was made of the tunnel when it had been excavated. The tunnel data was also combined with core data and geological mapping at the surface to produce a tectonic model of the site (Palmqvist and Lindström, 1988).

The borehole radar and the other borehole investigations have been performed by Swedish Geological Co. (SGAB). The tunnel investigations and the tectonic model were made by BERGAB - Berggeologiska Undersökningar AB.

This report contains a brief review of obtained results and the original radar model. The radar measurements were performed in December 1986 and since then considerable improvements have been made in processing and presentation of radar results. Therefore an updated radar model based on reprocessed data is also presented. The radar models are compared to the tectonic model and the tunnel data. An evaluation is made of the capabilites and limitations of the borehole radar method.

2 DESCRIPTION OF EXPERIMENTAL SITE

The experimental site is located at Huvudsta in Solna which is an urban district close to Stockholm (Figure 2.1). A blind road gives access to the site. The two boreholes ST1 and ST2 are situated at surface immediately above the extension of the tunnel. The borehole collars are separated by a distance of 2 m and the boreholes are directed away from each other (Figure 2.2). The plunge of both boreholes is about 60^{o} below the horizontal plane (Table 2.1). The coordinates of the boreholes are given in a local coordinate system with the X-axis being the length coordinate along the tunnel. Local grid north is perpendicular to the tunnel extension and is directed $N18^{o}E$ in relation to geographical north. The plane outlined by the boreholes is parallel to the tunnel extension. The tunnel is located at a depth of 60 m at the site, which means that the distance between the intersections of the two holes with the tunnel will be approximately 70 m.

The site is located at the boundary of a large gneissic outcrop close to a part of lake Mälaren. A fault striking NW and probably steeply dipping towards SW can be seen in form of a rock-face some tens of meters from the boreholes. ST2 is directed towards this fault.

Table 2.1 Borehole location and orientation in local grid coordinates.

		ST1	ST2
Bearing	(Deg.)	184.5	359
Plunge	(Deg.)	59.4	58.5
Position	X (m)	1736.26	1738.20
	Y (m)	-0.06	0.09
	Z (m)	3.34	3.46
Length	(m)	110	110

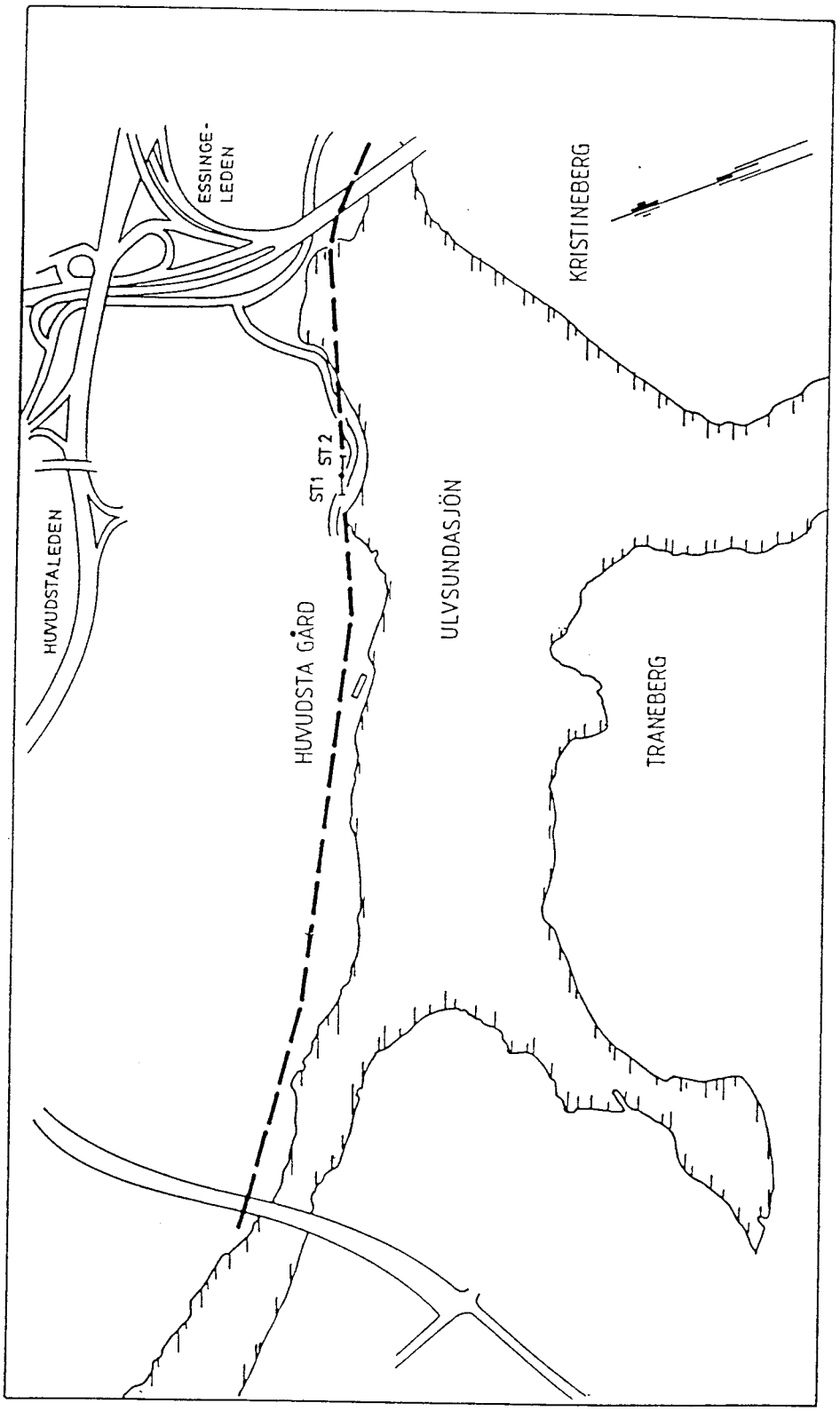

Figure 2.1 Location map of the Saltsjötunnel and position of boreholes ST1 and ST2. The tunnel is indicated by broken line.

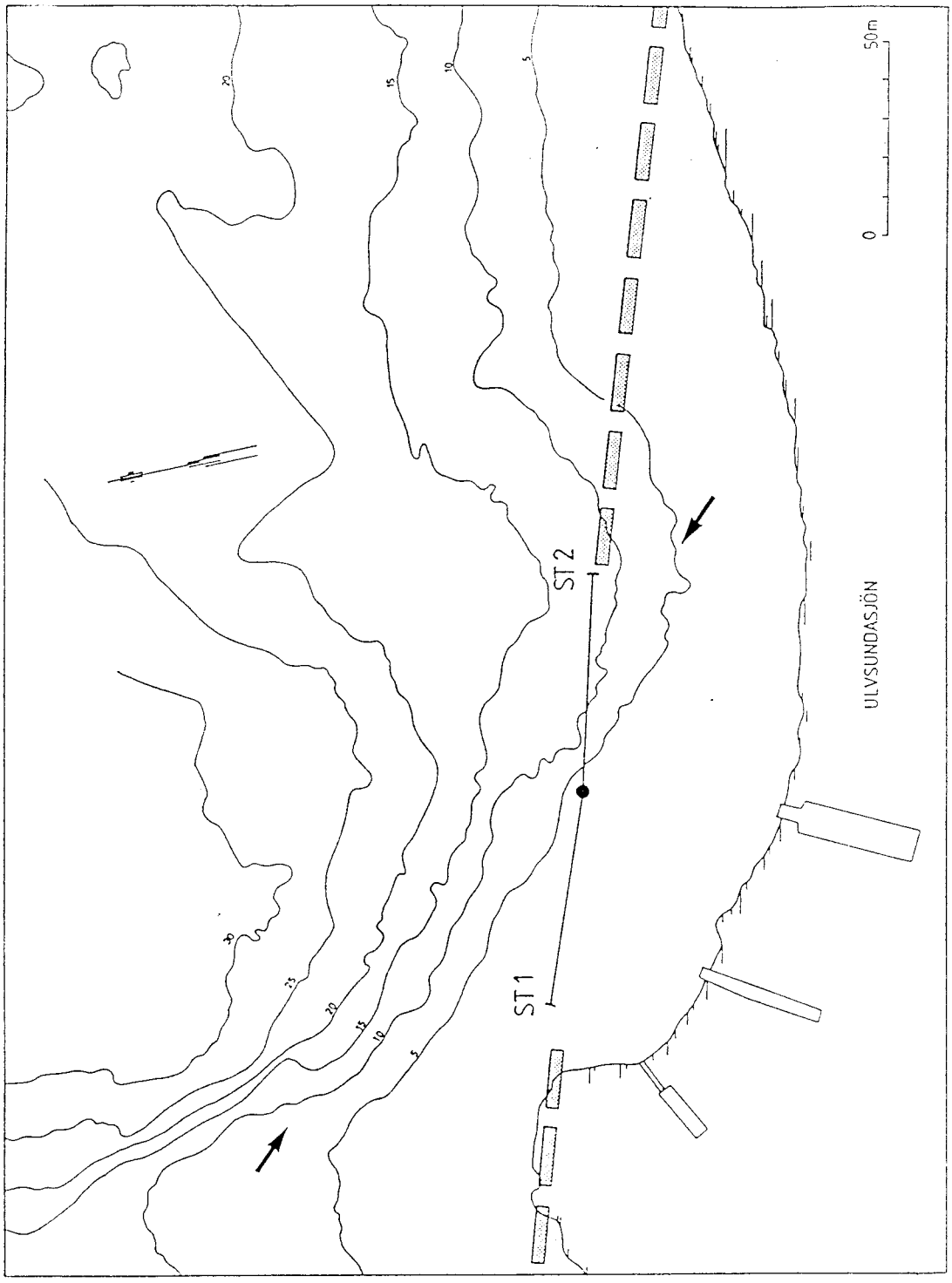

Figure 2.2 Detailed topographic map of investigated area and surroundings of boreholes ST1 and ST2 at the Saltsjötunnel. Arrows indicate steep rock-face.

3 INVESTIGATION PROGRAMME

The investigation programme started with borehole radar measurements in the two boreholes at the site. Single hole and crosshole measurements were performed with the centre frequencies 22 and 60 MHz.

The single hole reflection measurements are specified in Table 3.1. In a single hole measurement the borehole radar probe consists of a transmitter and a receiver separated by glass-fiber rods. The probe was in this case moved in 1 m steps. Sampling frequencies of 245.1 MHz and 494.1 MHz were used for the 22 MHz and 60 MHz measurements, respectively. A total of 344 m of single hole measurements were performed.

The crosshole measurements were also performed with the centre frequencies 22 MHz and 60 MHz (Table 3.2). The crosshole measurements were carried out by first having the transmitter fixed at the starting position 21.4 m in ST1, while the receiver was moved in 4 m steps between 21.4-105.4 m in ST2. After this scan of borehole ST2 had been completed the transmitter was moved 4 m downward and fixed at 25.1 m in ST1, and the next borehole scan was performed by moving the receiver in 4 m steps from 105.4 m to 21.4 m. The procedure was repeated until the transmitter had been located at all positions with a 4 m interval in the borehole section between 21.4 m and 100.4 m (bottom) in ST1. A total of 21 borehole scans each consisting of 22 rays thereby resulted in a total number of 462 rays for the frequency 22 MHz. 16 borehole scans each consisting of 22 rays gave a total of 352 rays for the frequency 60 MHz. The smaller number of rays for the 60 MHz measurement was due to the high attenuation which resulted in that no signal could be registered for the largest source-receiver separations. Hence measurement of the corresponding scans was not made.

The radar measurements were carried out during one week in the beginning of December 1986. The radar data were processed and interpreted. This interpretation was made without access to any other geological or geophysical data from the boreholes. The radar model was documented in a report which was completed January 19, 1987 (Carlsten, Falk, and Olsson, 1987). Hence, the project was set up as a "blind test" to check what information could be obtained from radar data only.

Table 3.1 Measured intervals from singlehole radar reflection measurements.

Frequency	ST1	ST2	Transmitter-receiver separation
22 MHz	11-96 m	19-100 m	15.4 m
60 MHz	9-97 m	8- 99 m	9.4 m
Step	1 m	1 m	

Table 3.2 Measured borehole intervals for crosshole tomographic measurements.

Frequency	ST1 Transmitter	ST2 Receiver
22 MHz	21.4-100.4 m	21.4-105.4 m
60 MHz	21.4-81.4 m	21.4-105.4 m
Step	4 m	4 m

After the radar model had been presented the boreholes were investigated in detail with other methods to check on the radar model and to complement it with new information.

Geological mapping of the core was made to describe variations in fracture frequency, identify fractured zones, and the lithology at the site.

Geophysical borehole logging was performed in order to characterize the physical properties of the rock at the site. The logs are used to identify fractured zones, lithologic units, and water flow to or from the borehole. The logging programme comprised the following methods:

- Natural gamma
- Single point resistance
- Normal resistivity
- Neutron
- Temperature
- Fluid resistivity

Hydraulic single hole injection tests were made in the boreholes to identify permeable sections. The entire length of the boreholes were logged with short-time tests using a packer spacing of 10 m. The permeable parts of the boreholes were tested with 2 m

packer spacing in order to characterize the permeable sections in greater detail and to define their location with greater accuracy.

Following the completion of the borehole testing programme an integrated evaluation was made of the borehole data. A number of fractured zones were identified in the boreholes. The borehole radar data was used to produce a model of the geometry of these zones. This model, made without access to any tunnel data, was presented in a report dated June 30, 1987 (Andersson, Andersson, Carlsten, Falk, Olsson, and Stråhle, 1987).

After excavation of the tunnel geologic and hydrologic mapping was made of the tunnel. The tunnel was mapped with respect to lithology, fracturing, and water inflow. The mapping data was also integrated with data collected during the excavation of the tunnel, e.g. grouting efforts. The tunnel data was, in conjunction with geological mapping data from the surface and the boreholes, used to construct a geologic-tectonic model of the site. This model is used as a basis for evaluating the capabilities of the borehole radar method. The tunnel mapping and the tectonic model is presented in a report dated August 31, 1988 (Palmqvist and Lindström, 1988).

The basic data collected and the different models produced have been compared and the borehole radar method evaluated. This is the object of the current report.

4 BOREHOLE RADAR

4.1 THE RAMAC SYSTEM

RAMAC is a short pulse borehole radar system. The system was originally developed by the Swedish Geological Co. (SGAB) as a part of the International Stripa Project. A continued development to make the system adapted for field work on a production basis has later been funded by SKB.

The radar system (RAMAC) consists of five different parts;

- a microcomputer with one 5 inch floppy disc unit and a 20 MByte harddisk for control of measurements, data storage, data presentation and signal analysis.
- a control unit for timing control, storage and stacking of single radar measurements.
- a borehole transmitter for generation of short radar pulses.
- a borehole receiver for detection and digitization of radar pulses.
- a motor-driven cable winch with an optical borehole cable for transmission of trigger signals to the borehole probes and data from the receiver to the control unit.

The RAMAC system works in principle in the following manner: A short current pulse is fed to the transmitter antenna, which generates a radar pulse that propagates through the rock. The pulse is made as short as possible to obtain high resolution. The pulse is received by the same type of antenna, amplified, and registered as a function of time. The receiver may be located in the same borehole as the transmitter or in any other borehole. From the full wave record of the signal the distance (travel time) to a reflector, the strength of the reflection, and the attenuation and delay of the direct wave between transmitter and receiver may be deduced.

The recording of the signal is similar to that of a sampling oscilloscope, i.e. for each pulse from the transmitter only one sample of the received electric signal is taken at a specific time. When the next pulse is generated a new sample is taken which is

displaced slightly in time. Thus, after a number of samples a replica of the entire signal is recorded. The sampling frequency and the length and position of the sampled time interval can be set by the operator.

Optical fibers are used for transmission of the trigger signals from the computer to the borehole probes and for transmission of data from the receiver to the control unit. The optical fibers have no electrical conductivity and will not support waves propagating along the borehole. Another advantage of optical fibers is that they do not pick up electrical noise and as the signal is digitized down-hole there is no deterioration of the signal along the cable. The quality of the results will thus be independent of cable length.

There is no direct connection between the transmitter and the receiver. Both probes are instead connected directly to the control unit and the transmitter and the receiver can be put into the same as well as into separate holes. In other words, the radar may be used for both single hole and crosshole measurements. The system also provides absolute timing of the transmitted pulses and calibrated gain in the receiver, which makes it possible to measure the travel time and the amplitude of the radar pulses in a crosshole measurement and hence provide data for a tomographic analysis. The absolute time depends on length of the optical fibers and is hence a quantity which has to be obtained through calibration for a given set of optical fibers. The block diagram of the control unit, transmitter and receiver is shown in Figure 4.1 and the technical specifications of the system are given in Table 4.1.

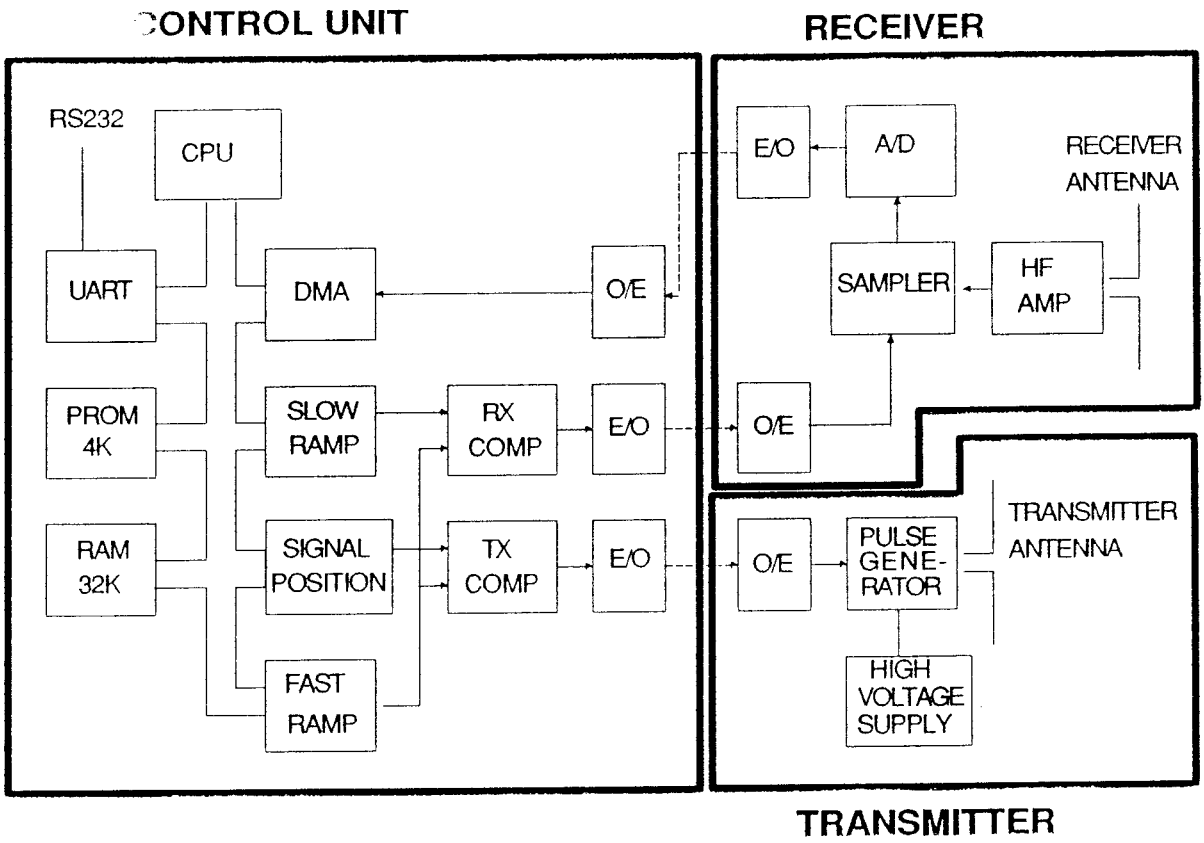

Figure 4.1 Block diagram of the RAMAC borehole radar system.

Table 4.1 Technical specifications of the borehole radar system.

General		
Frequency range	20-80	MHz
Total dynamic range	150	dB
Sampling time accuracy	1	ns
Maximum optical fiber length	1000	m
Maximum operating pressure	100	Bar
Outer diameter of transmitter/receiver	48	mm
Minimum borehole diameter	56	mm
Transmitter		
Peak power	500	W
Operating time	10	h
Length	4.8	m
Weight	16	kg
Receiver		
Bandwidth	10-200	MHz
A/D converter	16	bit
Least significant bit at antenna terminals	1	μV
Data transmission rate	1.2	MB
Operating time	10	h
Length	5.4	m
Weight	18	kg
Control unit		
Microprocessor	RCA 1806	
Clock frequency	5	MHz
Pulse repetition frequency	43.1	kHz
Sampling frequency	30-1000	MHz
No of samples	256-4096	
No of stacks	1-32767	
Time window	0-11	μs

4.2 MEASUREMENT CONFIGURATIONS

4.2.1 Single hole measurements

In single hole measurements the transmitter and receiver are located in the same borehole. The transmitter and receiver are kept at a fixed separation by glass-fiber rods. The transmitter-receiver array is moved along the borehole and measurements are made at fixed intervals. The measurement at each position takes about 30 seconds including the movement to the next measuring position. The separation of measurement points is normally 0.5 or 1 m.

4.2.2 Crosshole measurements

In a crosshole measurement the transmitter and receiver are placed in separate boreholes. The transmitter may also be kept at a fixed position on the ground while the receiver is moved in a borehole. This measurement configuration, with the transmitter on the ground, is termed Vertical Radar Profiling (VRP). The recorded signal may be analyzed both with respect to the travel time and amplitude of the first arrival and with respect to the occurrence of later arrivals such as reflections.

Crosshole measurements are carried out in the following way: one of the probes was kept at a fixed position in the first borehole while the other probe was moved in the other hole and measurements made with fixed increments. Such a set of measurements is termed a borehole scan. After each scan the probe in the first borehole is moved to the next position and the measurement in the second hole is repeated. This is repeated until the borehole section is fully measured. The separation of measurement points is normally 4-5 m for both fixed and moving probes when a tomographic survey is made. For crosshole reflection surveys the moving probe is normally moved in increments of 1 m while the separation of measurement points for the fixed probe is significantly larger.

4.3 PROCESSING AND INTERPRETATION OF RADAR DATA

4.3.1 Single hole reflection data

4.3.1.1 Interpretation procedure

The principle of a single hole reflection measurement is depicted in Figure 4.2. The transmitter and receiver are lowered or pushed into the same hole while the distance between them is kept constant. The result is displayed in the form of a diagram where the position of the probes is shown along one axis and the propagation distance along the other axis. The amplitude of the received signal is shown in a grey scale where black corresponds to large positive signals, white to large negative signals and grey to small signals.

The distance to a reflecting object is determined by measuring the difference in arrival time between the direct and the reflected pulse. The basic assumption is that the speed of propagation is the same everywhere. The two basic patterns are point reflectors and plane reflectors as shown in Figure 4.2.

From the radar reflection measurements it is possible to determine the angle of intersection between the hole and a fracture plane and also the point of intersection. This is done with the aid of a theoretically computed nomogram (Olsson, Falk, Forslund, Lundmark, and Sandberg, 1987). The information contained in the radar images is cylindrically symmetric as dipole antennas have been used due the small borehole diameter. Consequently one can not obtain the complete orientation of a fracture plane from measurements in a single borehole. The orientation can however be determined by combining results from two or more boreholes. In this multiple borehole analysis the possible orientations of a fracture plane are displayed as a curve in a Wulff diagram. There is one curve for each borehole measured and the intersection of the curves define the orientation of the zone.

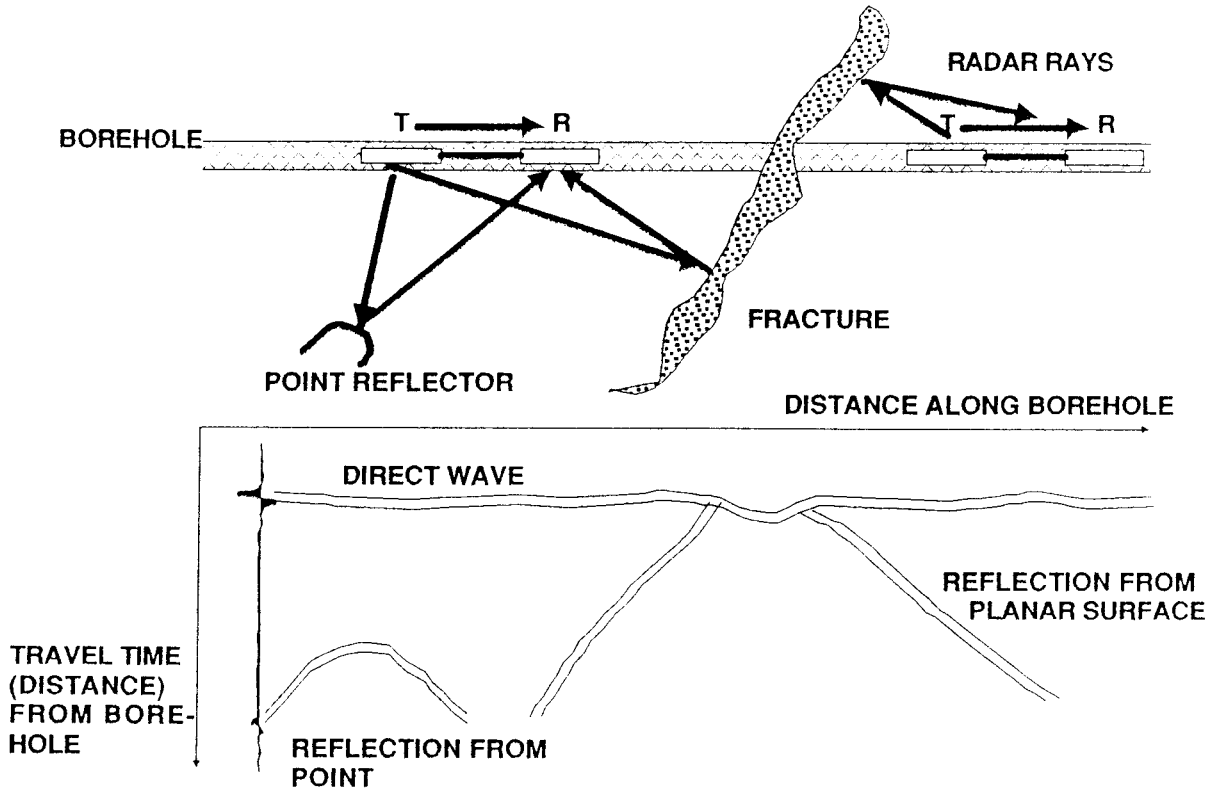

Figure 4.2 The principle of the borehole reflection radar and the characteristic patterns generated by plane and point reflectors.

4.3.1.2 Data processing

In many cases reflections from fracture zones and other inhomogeneities in the rock mass are not readily observed in the original radar data. In order to enhance reflections the radar data are digitally filtered.

A suitable filter for this purpose is the moving average filter. The filter is constructed so that the average is formed of a number of traces adjacent to the trace to be filtered and the average is subtracted from the centre trace. This is done for all traces along the borehole. With this type of filter, features on the radar signals which are similar for several adjacent traces will be removed. This includes the direct pulse as well as structures

nearly parallel to the borehole. The width of the filter, i.e. the number of traces included in the average, is chosen close to one wavelength.

4.3.2 Analysis of crosshole radar data

4.3.2.1 Tomographic analysis

Definition of the problem

The general idea behind tomographic reconstruction is that information about the properties of the interior of a region can be obtained through measurements at the boundary. In general the transmitter and receiver probes are located at the boundary of the area and each ray connecting transmitter and receiver can in principle be considered to represent the average of a measured property of the rock along the ray. In order to obtain an estimate of this property at a given point it is necessary that several rays pass close to the same point and that the rays have different directions and hence different information content. The requirement that several rays should intersect the same point puts some severe constraints on the borehole geometry. The main one being that the source and receiver positions and hence the boreholes have to be confined to the same plane.

In mathematical terms the tomographic problem can be formulated in the following way

$$d_i = \int_{T_i(m)} m(x) \cdot ds \qquad (4.1)$$

where d_i is the measured data for ray number i. The objective of the tomographic inversion is to estimate the spatial distribution of some property, $m(x)$, characteristic of the medium (x denotes the spatial location). The data is thought of as being a sum (line integral) of this property along the ray path, $T_i(m)$, from the transmitter to the receiver. The actual ray path is dependant on the properties of the medium, $m(x)$, and is normally the curve which gives the least possible travel time. The complex dependance of the ray paths, T_i, on the properties of the medium, $m(x)$, makes the problem nonlinear. The problem can be linearized by replacing the curves T_i with straight line segments, L_i, connecting sources and receivers.

In a borehole radar crosshole measurement data on the travel time and the amplitude of the direct wave between transmitter and receiver, i.e. the first arrival, can be extracted. It is assumed that the travel time can be constructed as the line integral of the slowness, s(x), along each ray.

The amplitudes can not be obtained from a line integral directly but the problem can be linearized by taking the logarithm of the data. The logarithm of the amplitudes can then be subject to tomographic inversion. The data used in the tomographic analysis are obtained from the measured amplitudes, E_m, according to the following equation

$$d_i = \int_{L_i} \alpha(x) \cdot ds = \ln \frac{c\, a(\theta_1)\, a(\theta_2)}{r\, E_m} \qquad (4.2)$$

where $a(\theta)$ is the antenna radiation pattern and 'c' represents a normalization constant describing the combined effect of transmitter power and receiver gain.

A discretization is made of the problem. The plane between the boreholes is divided into a number of cells and the line integral is calculated as a sum where the contribution from each cell is considered in proportion to the length of the ray within each cell, cf. Figure 4.3. A discretization of (4.1) transforms the equation into the following form

$$d_i = \sum_{j=1}^{M} G_{ij}\, b_j \qquad (4.3)$$

where G_{ij} represents the length of ray 'i' in cell 'j' and b_j the attenuation or slowness of cell 'j'.

The problem has now been transformed into a system of linear equations, where the number of equations correspond to the number of rays, N, and the number of unknowns, b_i, to the number of cells, M. Hence, we may write

$$\mathbf{d} = \underline{\mathbf{G}} \cdot \mathbf{b} \qquad (4.4)$$

This equation system can be both overdetermined and underdetermined at the same time and errors in the data may cause some equations to be in conflict. The most common solution concept for this type of equation is through minimization of the functional $|\mathbf{d}-\underline{\mathbf{G}}\cdot\mathbf{b}|^2$.

Normally the number of unknowns in the equation system is very large and iterative procedures will

have to be used to obtain the solution. The conjugate gradient (CG) method which was developed as a part of the Stripa Project is considered to be an efficient inversion procedure. The convergence is fast and hence few iterations are needed to arrive at the final solution. The CG-method has been shown to give smaller computing times and better reconstructions of model examples than the other iterative methods (Ivansson, 1984).

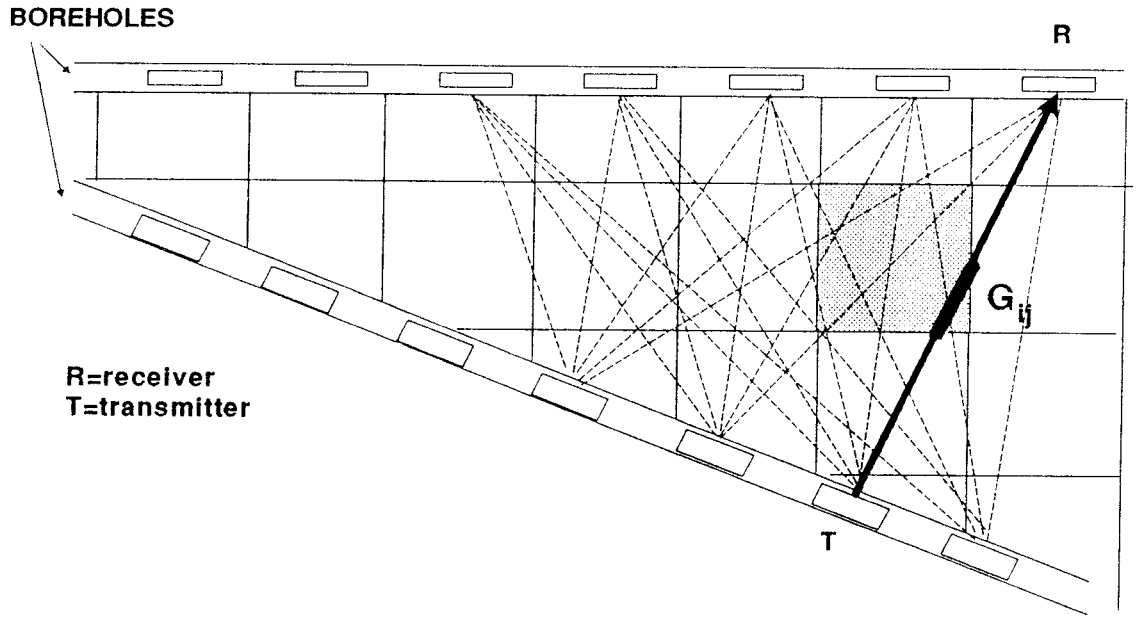

Figure 4.3 Generalized crosshole tomography geometry with a decomposition into cells and an example of a ray pattern.

Residual attenuation and velocity

The radar velocity (or slowness) has small variations around a certain average value. We have found it useful to put the crosshole data in such a form that these variations are studied rather than the absolute values of these properties. The concept has also been adopted for the amplitude data. In this context we define the terms 'residual travel time' and 'residual amplitude'. These residual data correspond to the measured data after subtraction of the expected data value which would have been obtained in a homogeneous medium with properties close to those of the investigated rock.

The residual travel time, t_r, is defined as the measured travel time, t_m, minus the estimated travel time for a homogeneous medium with a constant velocity, v_0. The residual travel time then becomes

$$t_r = t_m - r/v_0 \qquad (4.5)$$

where r is the distance between transmitter and receiver.

The residual amplitude is defined as the quotient (expressed in dB) of the received amplitude, E_m, and the estimated amplitude in a homogeneous medium with constant attenuation α_0. The residual amplitude, d_r, thus becomes

$$d_r = -20 \log_{10}\left(\frac{E_0}{E_m} \frac{\exp(-\alpha_0 r)\ a(\theta_1)\ a(\theta_2)}{r}\right) \qquad (4.6)$$

where E_0 represents a reference level corresponding to the ratio of transmitted power to receiver sensitivity. Through the use of the base 10 logarithm and the multiplication by 20, the residual amplitudes become represented in dB.

With this conversion into residual data it is possible to look at small variations from large average values. The residual data are also suitable for detecting systematic errors in the data and can be used for calibration of some system parameters.

Travel time and amplitude picking

A typical example of a radar signal recorded from a crosshole measurement is shown in Figure 4.4. From this signal trace we want to obtain the time of first arrival and the magnitude of the signal.

A tomographic survey normally includes a large number of rays. It is therefore of utmost importance to arrive at some automatic procedure which can pick the data from the recorded traces, especially as a manual treatment of each ray would be extremely time consuming and hence costly. For the radar data we have adopted a simple approach which in a number of cases has proven to be reasonably efficient. An algorithm has been devised which picks out the maximum and the minimum for each trace and the time instances at which these events occur. The travel time is then defined as the time to the maximum or minimum of the pulse and the amplitude is defined as the difference between the maximum and the minimum, i.e. peak-to-peak amplitude.

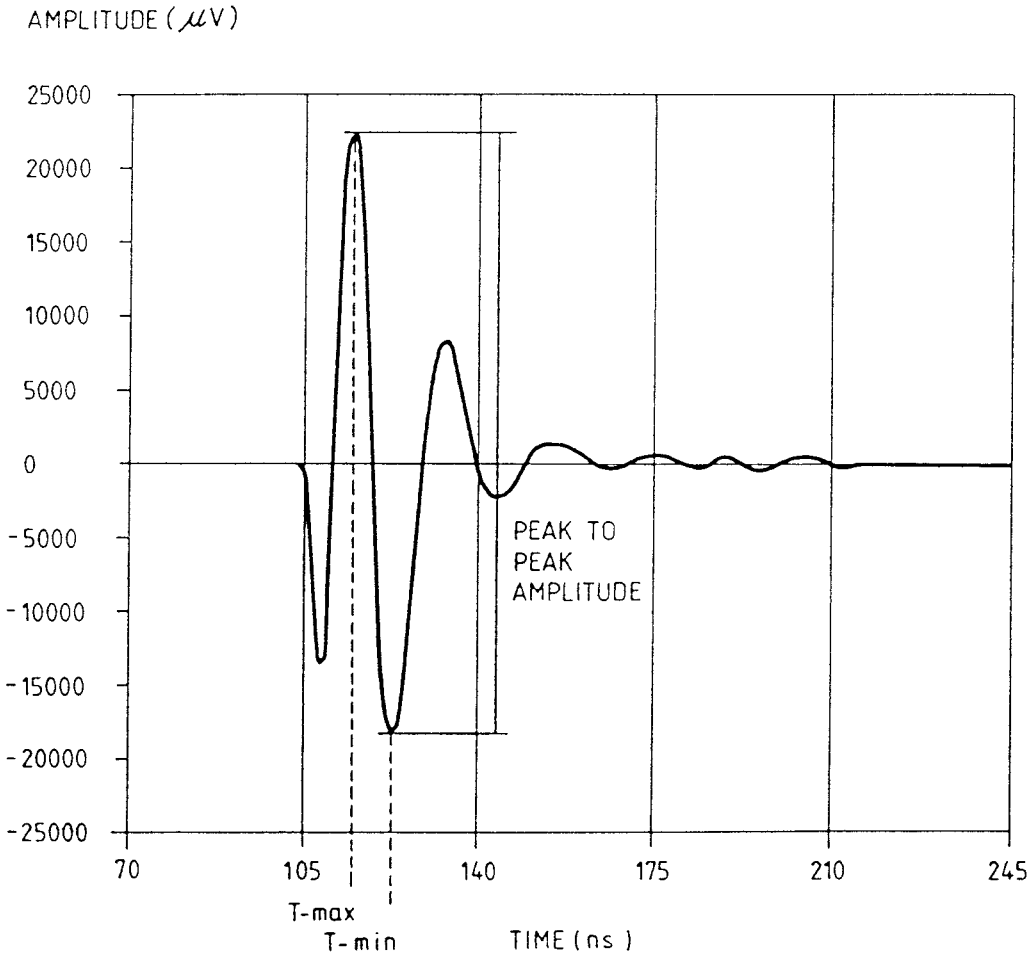

Figure 4.4 Radar signal obtained from a crosshole measurement. The data identified by the automatic routine for extraction of travel times and amplitudes are indicated.

Attachment of coordinates to data

The basic step in preparing data for tomographic inversion is the attachment of coordinates to the picked travel times and amplitudes. The accuracy required in source and receiver coordinates is of the same order as the propagation distance during a sampling interval. The sampling interval normally corresponds to a propagation distance of 0.2-0.5 m.

After the travel time and amplitude data have been combined with the coordinates of the source and receiver points the residual data are calculated according to (4.5) and (4.6).

Data quality checks and corrections - general remarks

The tomographic data is subject to a number of errors such as; errors in time and amplitude picking, constant offset errors in time and gain, and coordinate errors. It is essential to get a grasp of both the stochastic and systematic errors which may exist in the data set. The errors must be understood, quantified and corrected before a tomographic inversion is attempted. A good way to reveal errors is to plot the residual data as a function of the length of the rays. From these plots an offset and a slowness or attenuation correction is determined. A grey scale plot (or ray check plot) is then made of the average slowness or attenuation for all rays. In this plot individual rays containing errors (e.g. due to errors in time and amplitude picking) can be identified. Rays containing errors are removed from the data set before tomographic inversion.

The data correction and quality checking procedure is described in detail by Olsson, Falk, Forslund, Lundmark, and Sandberg, 1987.

Tomographic inversion procedure

The tomographic inversion is made with the iterative Conjugated Gradient (CG) method described by Ivansson (1984).

The inversion is normally made with rectangular basis functions, i.e. the velocity of each cell is assumed to be constant within that cell. A cell size of approximately 3 m is normally used.

4.3.2.2 Crosshole reflection analysis

When the transmitter and receiver are positioned in different boreholes, reflected pulses are observed some time after the directly propagated pulse has arrived. Only the direct pulse is used in the tomographic analysis, so the crosshole reflections provide additional independent information about the fracture zones. This method has provided complementary information on the orientation of the fracture zones identified in the single hole reflection data and the tomograms.

It is particularly convenient that crosshole reflections in principle can determine a complete orientation of a fracture zone. This is due to the additional freedom provided by a bistatic radar configuration. The analysis is however more complicated than for single hole measurements. In the following section the method of analysis is presented in some detail.

The bistatic radar configuration is defined in Figure 4.5. The receiver and transmitter are in known positions described by the vectors $\mathbf{x}_0$ and $\mathbf{x}_1$. The distance l propagated by the direct pulse and the distance l′ propagated by the reflected pulse are then conveniently combined into the expression

$$l'^2 = l^2 + 4(\mathbf{x}_0\ \mathbf{n})(\mathbf{x}_1\ \mathbf{n}) \qquad (4.7)$$

where $\mathbf{n}$ is the unit normal vector of a plane causing the reflection. The formula is valid as long as the origin is in the reflecting plane. One such point can be determined from the radar picture, since l=l′ when the antenna passes that point where the fracture plane intersects the borehole. Using this point as an origin one can then proceed to analyze the reflection. A detailed derivation of the formula is found in Olsson, Falk, Forslund, Lundmark, and Sandberg, 1987.

The reflection curves are digitized and analyzed in a special program. In principle all quantities in the formula can be obtained from the measured data, so the two independent components of the unit vector $\mathbf{n}$ can be determined from a minimum of two separate measurements. This should be compared with the special case of a single hole measurement where the receiver and the transmitter are moved along the same borehole. The angle between the fracture plane and the borehole can then be determined immediately but no more information about the orientation of the plane is available due to the axial symmetry of the single hole configuration.

The crosshole configuration in principle provides complete information about **n**, but the results can not be directly interpreted as orientation angles. Instead we obtain a "slope", the quantity $(\mathbf{x}_0 \cdot \mathbf{n})(\mathbf{n} \cdot \mathbf{t})$ appearing in the formula 4.7 (**t** is here the unit vector along the borehole).

The formula 4.7 can be used to plot the possible orientations of a zone for every reflection identified with it. Performing the same procedure for several different crosshole measurements one obtains a number of curves all intersecting each other near some point corresponding to the correct orientation. This procedure is very similar to the one used for analysis of single hole reflection data.

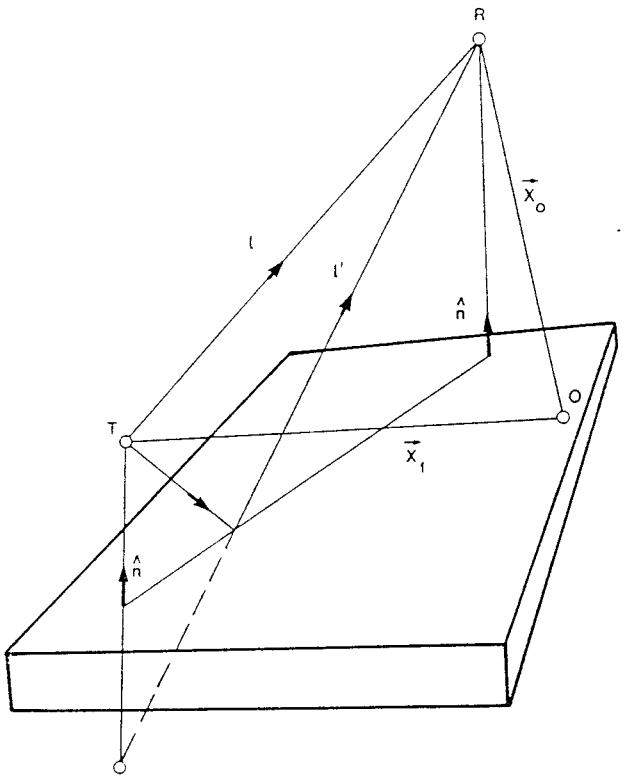

Figure 4.5 Principal ray paths in a bistatic radar configuration where the ray is reflected in a plane. T = transmitter, R = receiver, l = direct wave, l′ = reflected ray, $\mathbf{x}_0$ = location vector of receiver, $\mathbf{x}_1$ = location vector of transmitter, **n** = normal vector to plane.

5 PREDICTIONS BASED ON BOREHOLE RADAR

5.1 THE ORIGINAL RADAR MODEL

The original radar model of the site was obtained mainly from a combination of the data from the single hole reflection measurements and the results of the amplitude tomography. The results from the crosshole reflections did not contribute much to the construction of the radar model due to the high attenuation at the site.

The radar reflection results are shown in Figures 5.1-5.4. The radar reflection data have been processed with a moving average filter this is a filter which suppresses reflectors which are parallel to the borehole. Parallel reflectors are often caused by inadequacies of the instrument. Hence, the moving average filter is effective in suppressing instrument noise and will enhance reflections caused by structures in the rock mass. In these figures the reflections identified have been indicated and numbered.

The 60 MHz radar map from ST1 exhibits 16 reflections with small angle (20-35^{o}) to the borehole axis (Figure 5.1). A majority of the reflections are more or less parallel to each other thus indicating a pattern of parallel structures in the rock mass. One reflector (no. 2) in the radar map has a significantly different orientation, namely 50^{o} to borehole axis. This reflection was interpreted to represent a part of a subhorizontal structure.

The 22 MHz radar map from ST1 exhibits a similar pattern of structures with a small angle to the borehole axis (Figure 5.2). However, one reflection exhibits an angle of 50^{o} to borehole axis, this corresponds to a similar reflection in the 60 MHz radar map.

The 60 MHz radar map from ST2 exhibits 17 reflections which all are interpreted as vertical or subvertical structures (Figure 5.3). The 22 MHz radar map from borehole ST2 exhibits a similar pattern of structures with acute angles to the borehole axis (Figure 5.4). Exceptions are two reflections which have a somewhat larger angle of 40^{o} to borehole axis (nos. 3 and 9). Both structures are interpreted as representing parts of a subhorizontal structure.

There are sections along the boreholes which exhibit loss of radar pulse energy. These sections occur in all four radar maps, and they are interpreted to represent a subhorizontal structure denominated A. The energy loss indicates a highly attenuating zone a few metres wide intersecting borehole ST1 at 35-39 m and ST2 at 42-45 m. At 62-65 m in ST1 there is also a similar but weaker section in the 22 MHz data which might represent a part of a vertical structure, B. The orientation of this structure was deduced from the single hole reflection data. The reflections associated with these sections are rather weak and are sometimes not seen at all.

A majority of the singlehole reflections intersect the boreholes with an angle in the interval 25-35^{o}. Most of these reflections are more or less parallel to each other and consequently they are considered to represent a common characteristic of the rock mass such as a prevalent fracture orientation.

A plot in a Wulff net of the singlehole data gives three possible orientations for this set of radar reflectors; one set striking roughly N-S (in the local grid system) with an almost vertical dip, two sets striking E-W (local grid) with dips of about 50^{o} towards north and south, respectively. Taking the following description of the tomograms and singlehole radar into account, the first vertical set is considered best suitable.

The result of the singlehole radar measurement were combined with the tomographic maps obtained from the crosshole measurements. The tomograms obtained in January 1987 are shown in Figures 5.5 and 5.6 which also show the resulting radar model. It should be noted that the presented radar model is a conciliation of the interpretation of the tomograms and single hole reflection radar, and smaller discrepancies might occur.

Structure A appears as a nearly horizontal feature in the tomograms. It is interpreted as being the structure connecting the part of the borehole where the radar pulse energy losses are significant in the singlehole reflection measurements, but the structure does not exhibit distinct reflections in ST2. The crosshole data shows that the structure is penetrated by both boreholes at the depth interpreted from the single hole measurements. It has not been possible to determine the dip of structure A with any accuracy but the most probable interpretation is that the structure is semihorizontal.

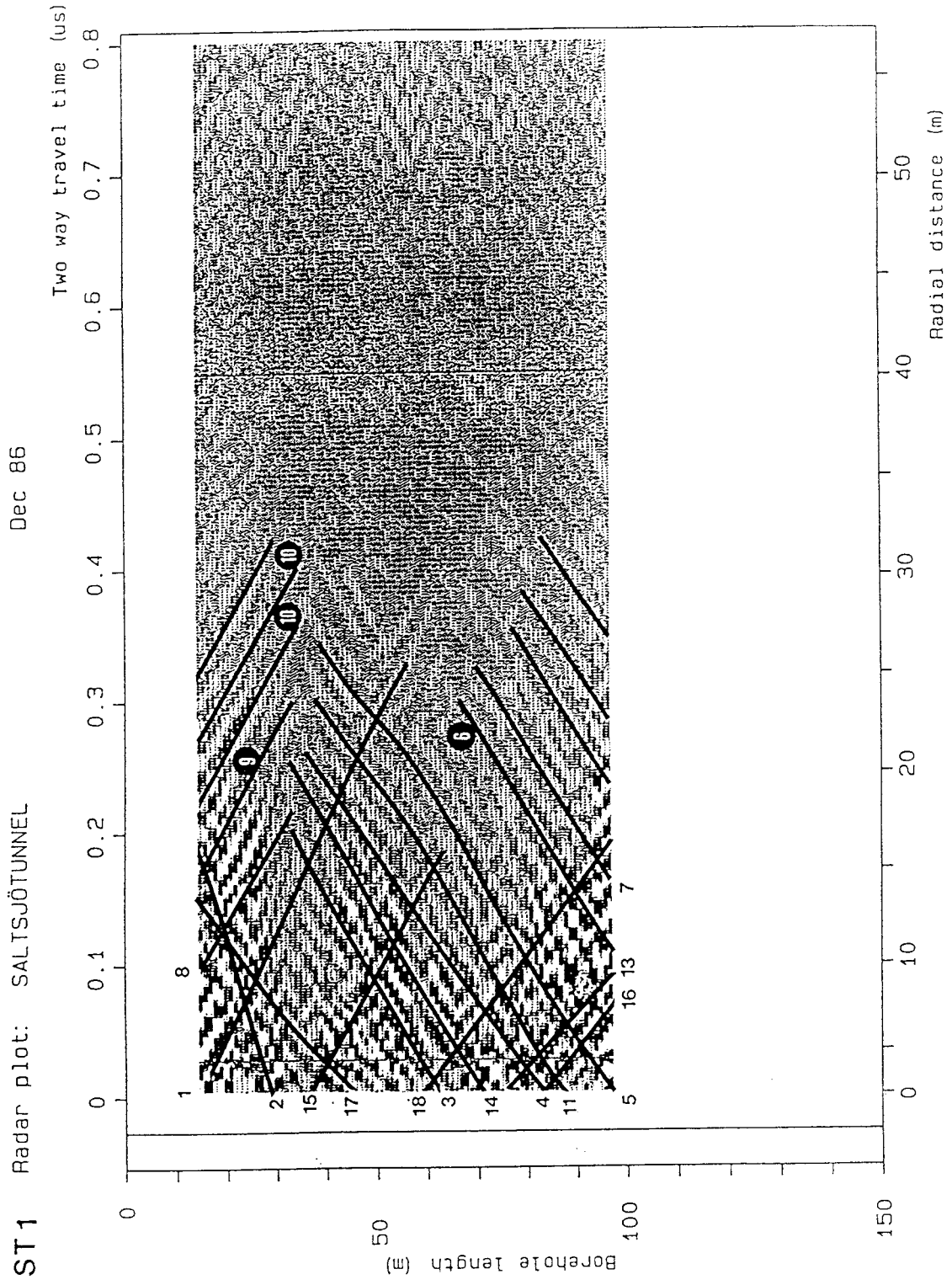

Figure 5.1 Radar reflection map for borehole ST1.
Centre frequency 60 MHz.

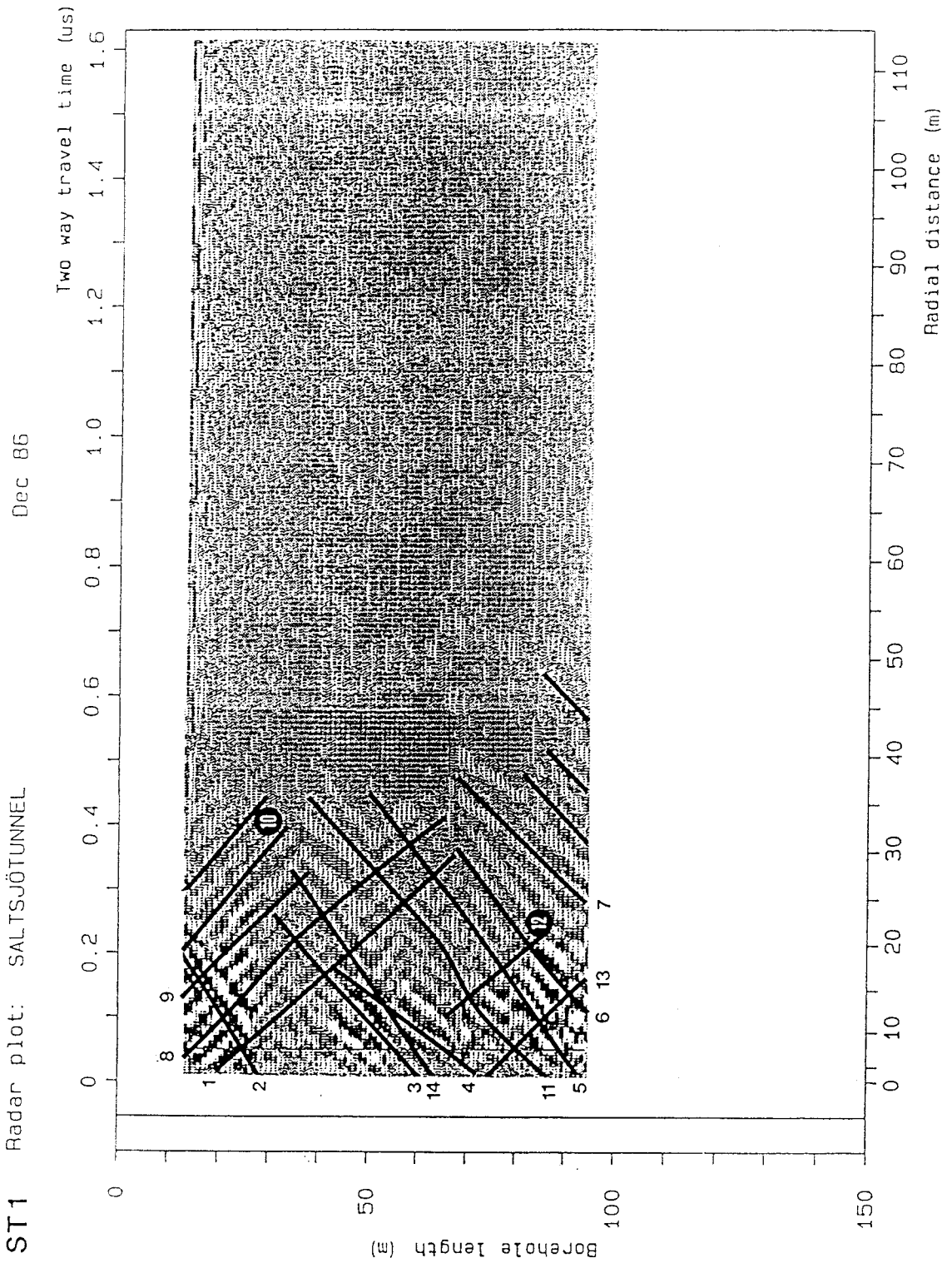

Figure 5.2 Radar reflection map for borehole ST1.
Centre frequency 22 MHz.

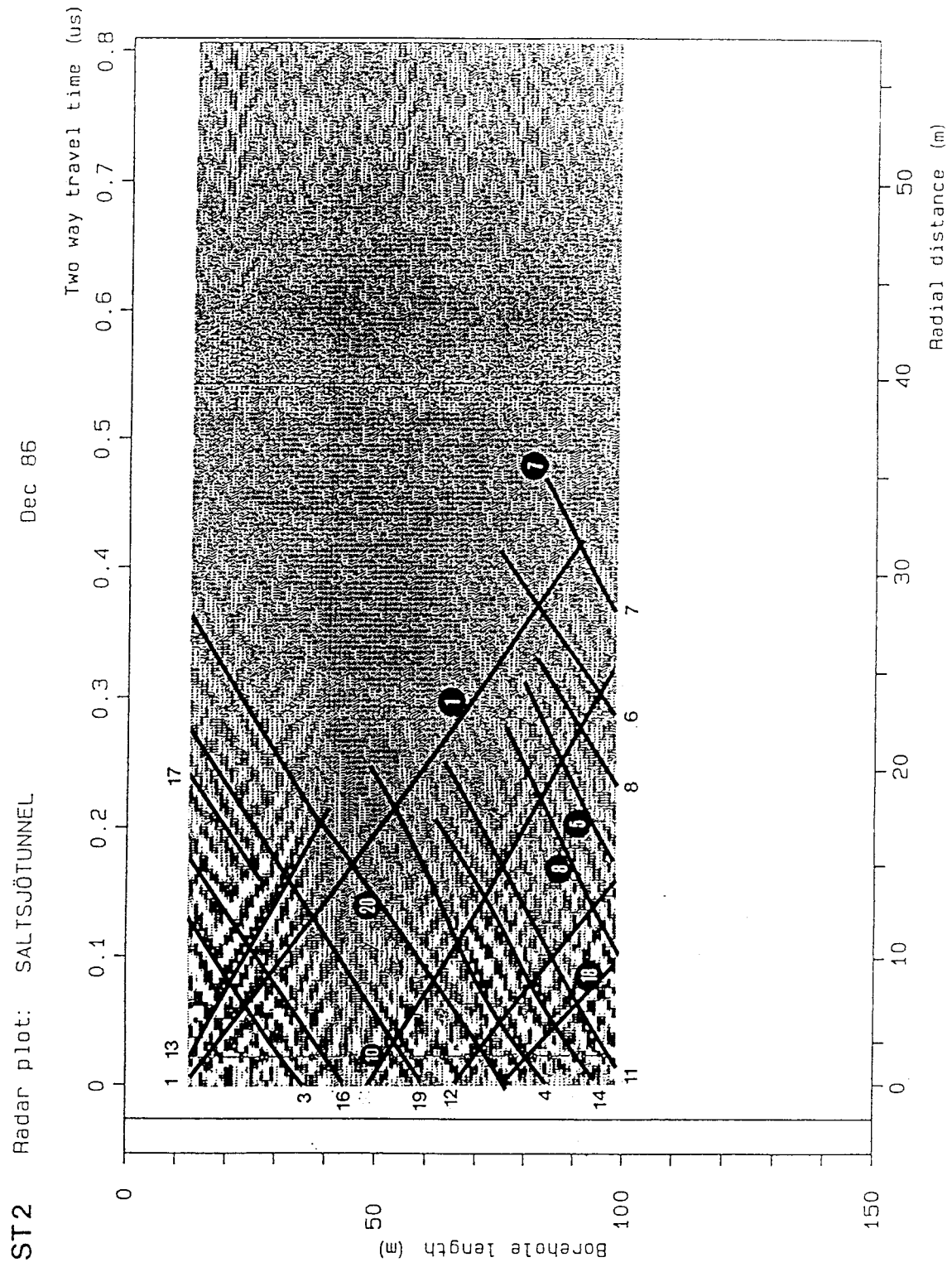

Figure 5.3 Radar reflection map for borehole ST2.
Centre frequency 60 MHz.

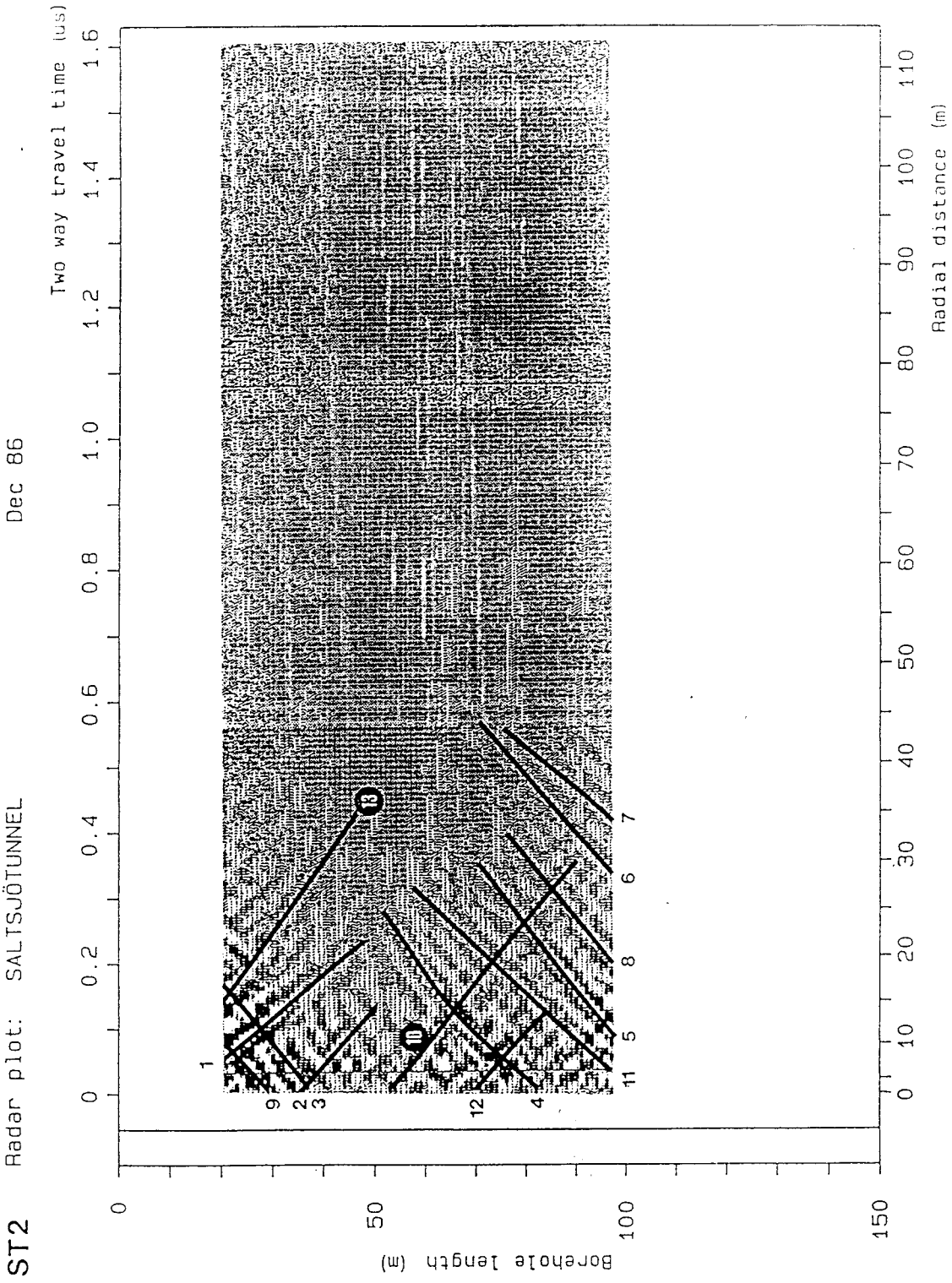

Figure 5.4 Radar reflection map for borehole ST2.
Centre frequency 22 MHz.

Structure B appears with a steep dip in the tomogram. The intersection with borehole ST1 between 50-63 m is determined from the singlehole reflection measurement. The most probable strike of the structure is NW which roughly corresponds to a marked feature in the topography.

In the tomogram structure C seems to have a steep dip above a vertical depth of 50 m and below that depth the dip is reduced. The crosshole reflection data indicates a slightly different location and orientation for the structure. From that data it appears to intersect ST2 at a depth of 25-35 m and to have a dip of about 60^{o}. From the singlehole reflection measurement this section is represented by one reflection, namely no.2 (22 MHz) indicating a dip of 35^{o} to borehole axis. The strike of the structure should be approximately perpendicular to the plane of the boreholes. A dip of 60^{o} is roughly in correspondence with the dip indicated in the tomogram at a depth below 50 m. The crosshole reflection data also indicate that at least two structures with different orientations intersect ST2 at about 40 m.

Based on the results from the singlehole reflection data structure D is thought to be steeply dipping. It can be assumed that it is more or less parallel with structures B and C.

Structure E appears with a steep dip in the travel time tomogram. It can be treated as parallel to structure B. Its existence is supported by the 60 MHz single hole measurement as two reflections intersecting at 74 m in ST1, with an angle of 25^{o} and 18^{o}, respectively. This would imply a vertical dip of the structure.

A general feature of the obtained tomograms is the relatively larger attenuation and slowness in the Western part of the investigated borehole section between structures B and C.

The attenuation of the radar waves at this site is considerably higher than what has been obtained at most other radar investigated sites. This generally indicates a high level of fracturing and alteration. In this area, the high attenuation is probably related to the complex rock mass containing several contacts between different rock types.

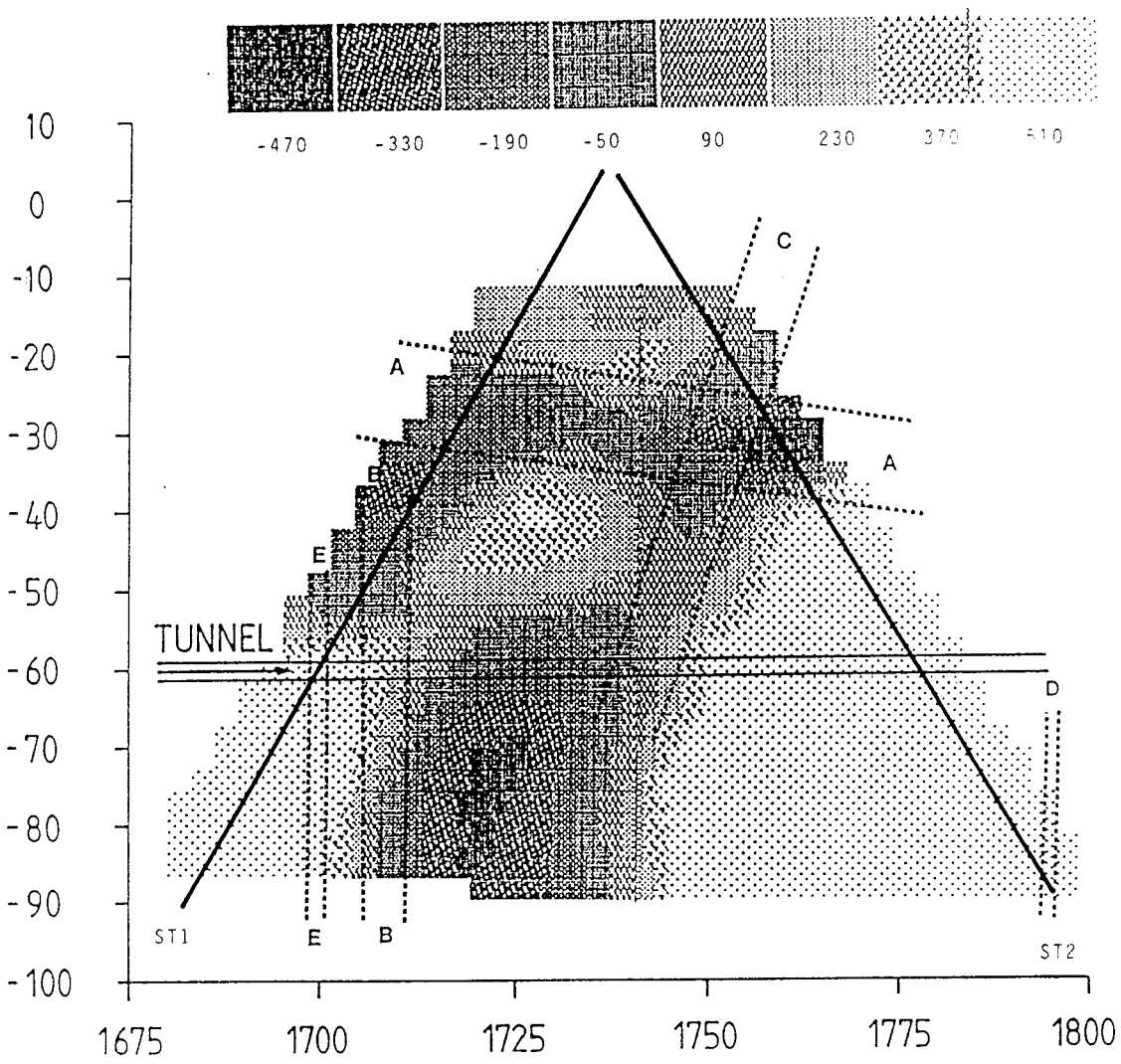

Figure 5.5 Original radar tomogram showing the distribution of attenuation in the plane between the boreholes ST1 and ST2 at a centre frequency of 22 MHz. Major features included in original radar model are indicated.

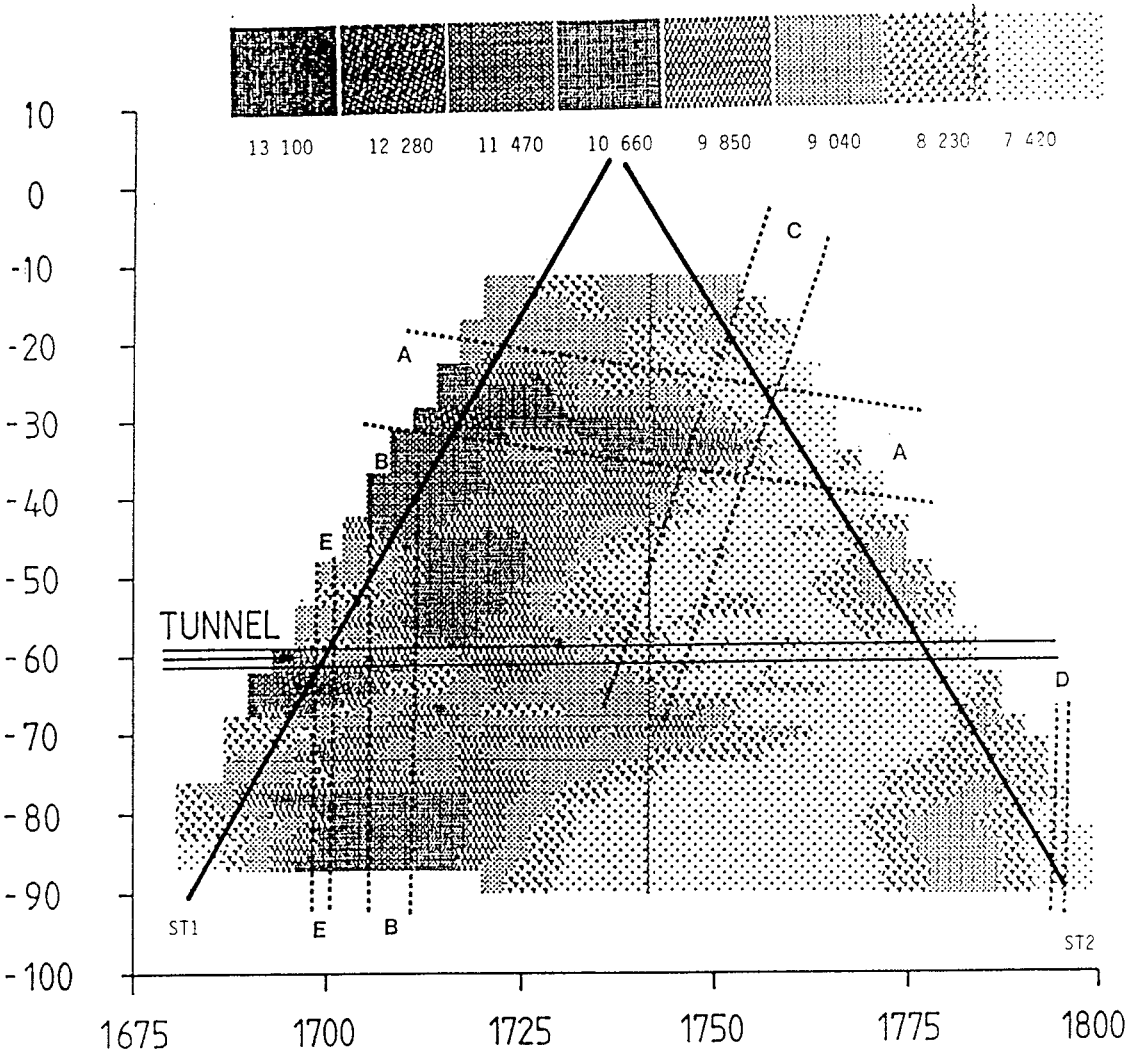

Figure 5.6 Original radar tomogram showing the distribution of slowness (inverse velocity) in the plane between the boreholes ST1 and ST2 at a centre frequency of 22 MHz. Major features included in original radar model are indicated.

5.2 REVISED RADAR MODEL

During the time since the original radar processing and interpretation was made significant improvements have been made in techniques for processing of radar data. The greatest achievements in processing techniques have been made with respect to the tomographic inversion algorithm. The tomographic inversion algorithm that had been used for producing the original tomograms (Figures 5.5 and 5.6) caused significant artifacts especially in regions with low ray density. The artifacts were caused by the tendency of the algorithm to concentrate the effects of data errors into regions of low ray density. Artifacts were also caused by the smoothing or damping applied to the solution.

Smoothing of the solution is applied to average the effect of data errors. The basic assumption in the smoothing algorithm is that the properties of adjacent cells should be similar. Hence, the rock is assumed to show a certain degree of continuity with respect to its properties. However, in the original algorithm the weight of the smoothing was assumed to be the same over the entire area covered by the tomogram. It was realized that the applied smoothing in some cases lead to unrealistic results (Olsson, in press). One example of this is the large attenuation anomaly in the bottom of the tomogram, approximately at the tunnel coordinate 1/725. A comparison of the tomogram with the ray pattern (Figure 5.7) shows that the lower region only contains rays that are essentially parallel. This implies that the rays contain no information which identifies the location of the anomaly along these rays. Hence, the anomaly appearing at 1/725 does not reflect the information content of the data and must be an effect of the tomographic inversion algorithm applied. To remove this problem and to obtain a tomographic solution which reflects the information content in the data, i.e. anomalies are well defined in regions of high information content and smeared out in regions of low information content, a new tomographic inversion algorithm has been developed where the weight of the smoothing equations is dependant on the ray density within each cell (Olsson, in press).

The new tomographic algorithm has been applied to the data from ST1 and ST2. Figure 5.8 shows a map of the ray density. It can be observed that the ray density is low in the lower part of the mapped area and in a small region at the top. The resulting travel time and attenuation tomograms are shown in Figures 5.9 and 5.10. Anomalies in the lower part of the tomograms are now smeared in the horizontal direction

reflecting that rays in this part are nearly horizontal.

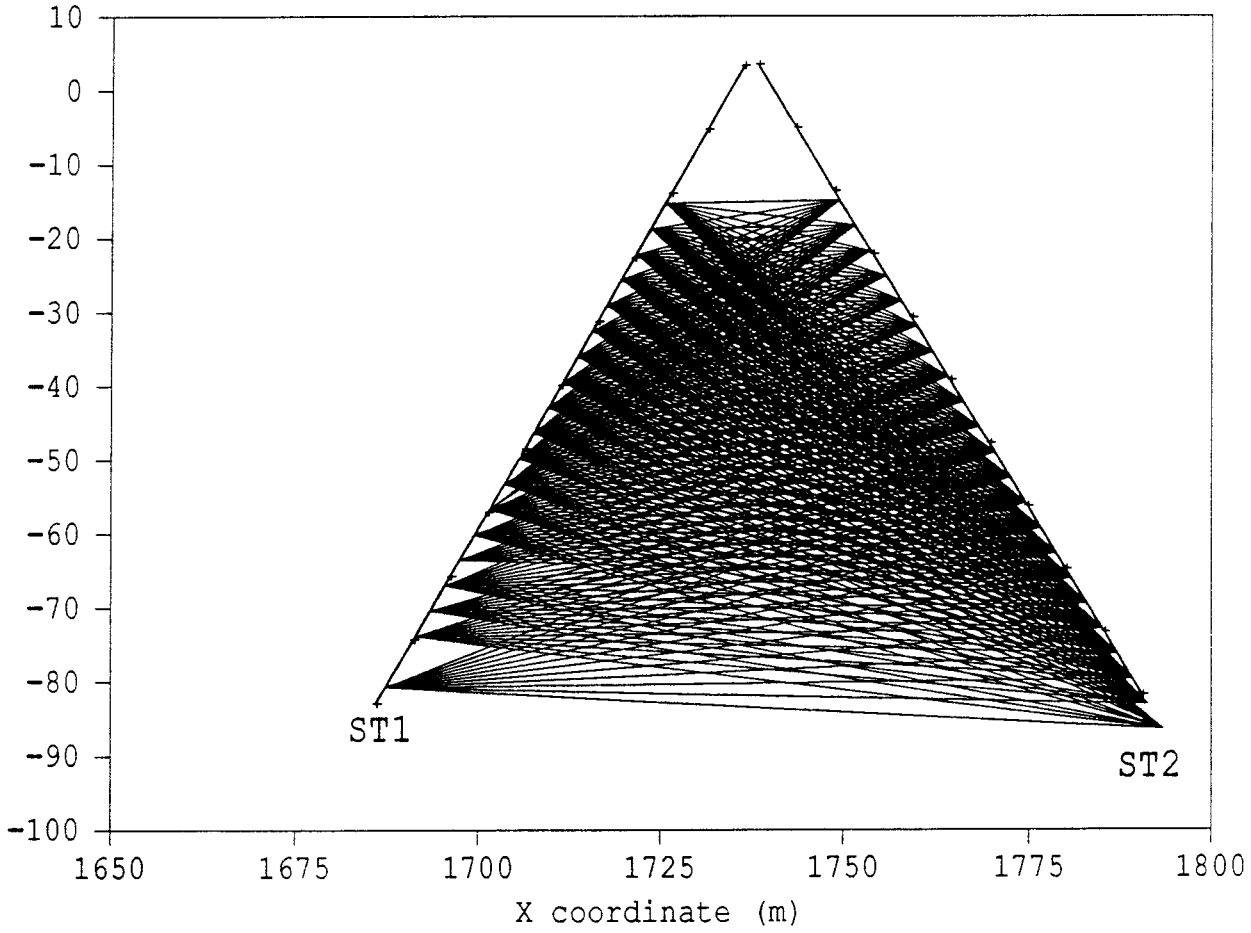

Figure 5.7 Ray pattern used for the generation of slowness and attenuation tomograms in the ST1-ST2 plane.

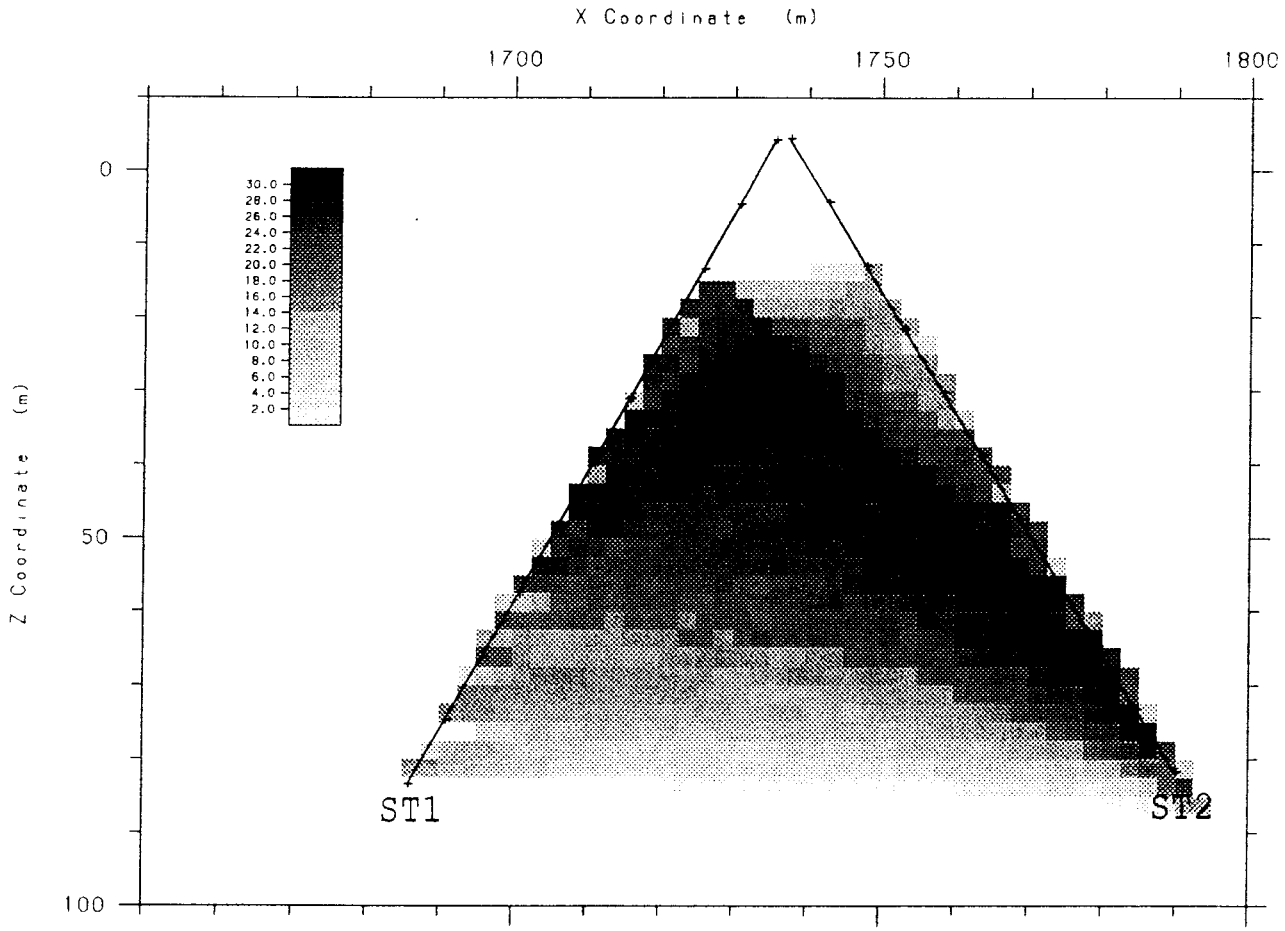

Figure 5.8 Map showing the number of rays per cell used for generation of slowness and attenuation tomograms of the ST1-ST2 plane.

The new tomograms are significantly different from the original tomograms and a revision of the interpretation based on the tomograms is warranted.

A comparison of the old tomograms (Figures 5.5 and 5.6) and the new ones (Figures 5.9 and 5.10) indicates that the only anomaly which remains the same is the feature A. Features B and C vanish completely while there are both a slowness and an attenuation anomaly associated with feature E.

Hence, the new tomograms give an impression of the geologic conditions at the site which is different from the original one in several important aspects.

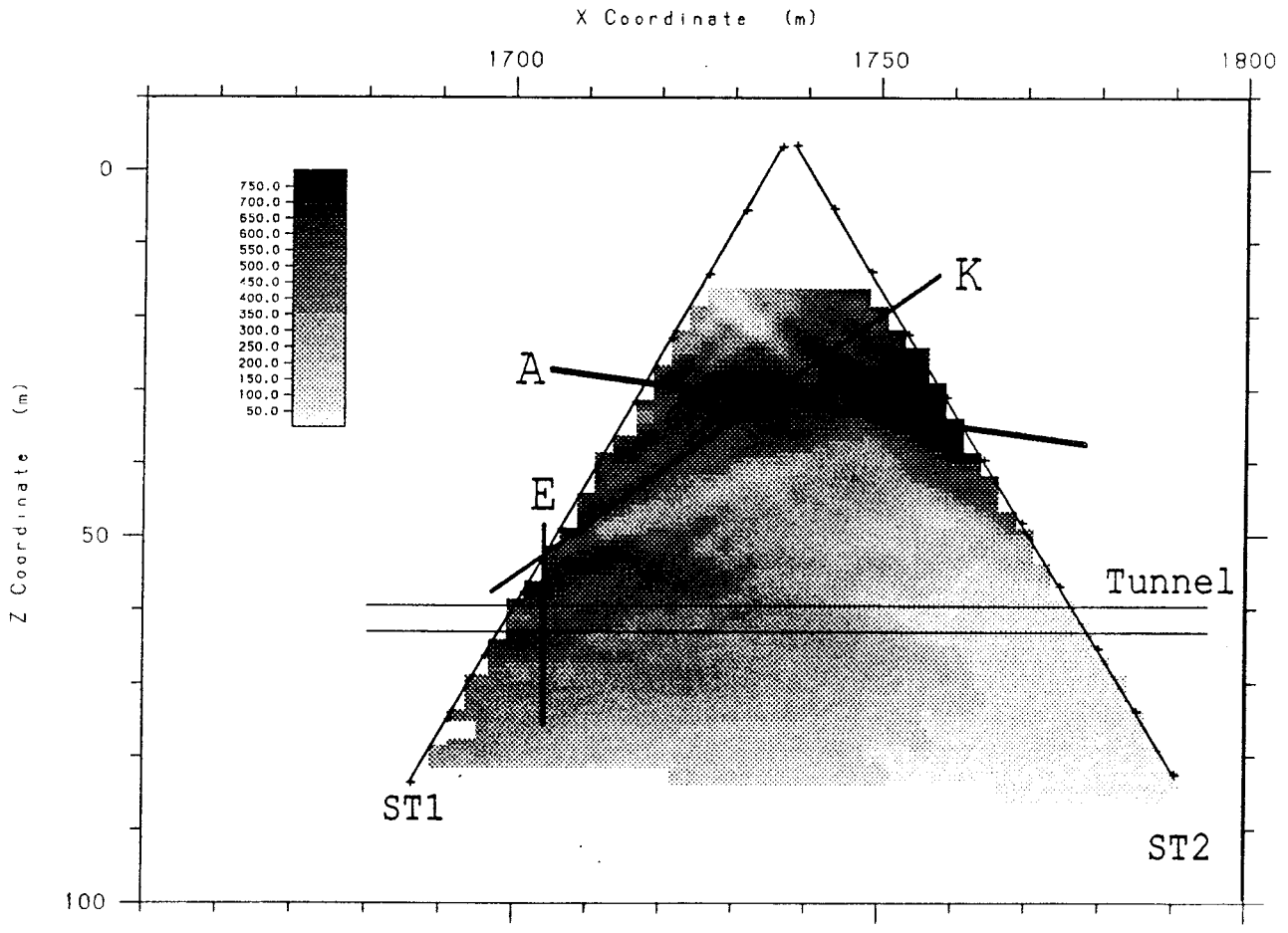

Figure 5.9 Radar attenuation tomogram of the ST1-ST2 plane obtained with the new inversion algorithm. Centre frequency 22 MHz. Major features included in revised radar model are indicated.

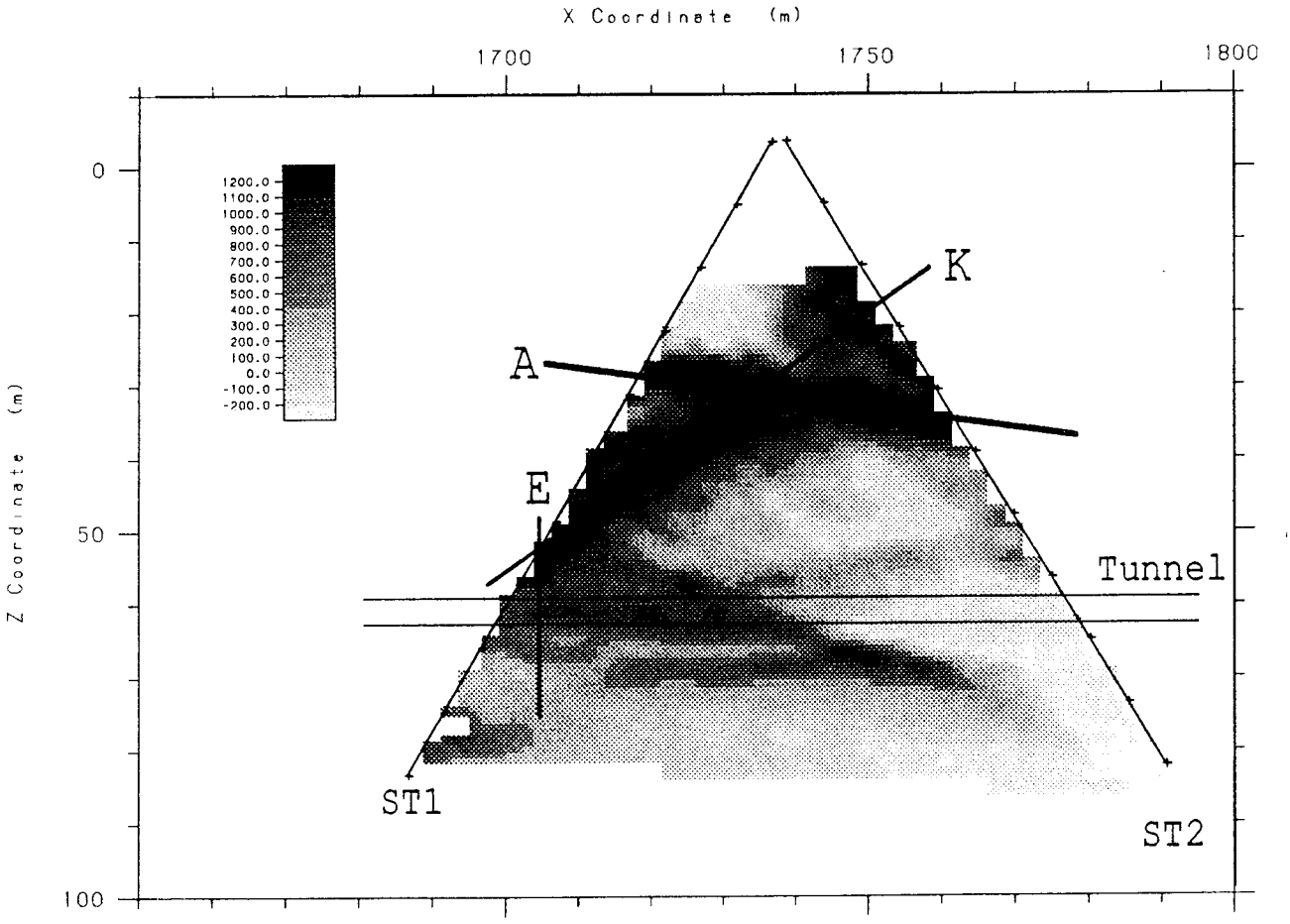

Figure 5.10 Radar slowness tomogram of the ST1-ST2 plane obtained with the new inversion algorithm. Centre frequency 22 MHz. Major features included in revised radar model are indicated.

The revised radar model consists of the following features:

- A major subhorizontal feature named 'A'. It has a dip of 10 to 15 degrees in the ST1-ST2 plane. It is the most significant slowness and attenuation anomaly at the site. It causes radar reflections of moderate strength in ST1 while reflections are difficult to observe in

St 2. The radar reflection data indicate a dip of 40° either to the North or to the South.

- Both tomograms indicate anomalous electrical properties at a borehole depth of about 67 m in ST1. The slowness tomogram indicates a structure, 'K' with a dip of approximately 35° in the ST1-ST2 plane while the feature is only weakly indicated in the attenuation tomogram. In combination with the reflection data this indicates a structure with a strike perpendicular to the tunnel dipping 35°W. The increased attenuation and slowness observed at approximately 20 m borehole length in ST2 is also assumed to be associated to this feature.

- The radar reflection data indicate a number of smaller features, probably corresponding to a dominant fracture orientation, striking roughly N-S and with a vertical dip. These features give rise to numerous but weak reflections and should be seen as representations of some common characteristic of the rock mass, such as a dominant fracture orientation rather than some definite feature. A few strong reflectors with this orientation is found in the interval 60-80 m in ST1. This corresponds to the previously identified feature 'E'.

It should be noted that the revised radar interpretation gives no support for the existence of the features 'B', 'C', and 'D' contained in the original radar model.

6 RESULTS FROM TUNNEL INVESTIGATIONS

6.1 GENERAL

In order to make it possible to evaluate the predictive capabilities of the borehole radar technique a geological-tectonic model has been constructed. The construction is based on drill core mapping of the investigation holes ST1 and ST2 and a mapping of the relevant part of the tunnel. Strike and dip of structures and fractures around the boreholes have also been measured in order to, if possible, determine the orientation of structures and fractures in the core.

6.2 GEOLOGICAL CHARACTERIZATION

6.2.1 Bedrock conditions at the site

The site consists essentially of two rock types, grey fine to medium grained granite and grey medium to coarse migmatite. The granite, i.e. the Stockholm granite, is homogeneous and shows only weak foliation. The migmatite, i.e. migmatite gneiss, is veined and rather coarse. The origin is presumably a greywacke. According to the regional geological map the strike of the migmatite in the investigation area and its surroundings is NNW and the dip 80-85^{o} towards East (Stålhös, 1969).

6.2.2 Core mapping

Stockholm granite dominates the boreholes. The granite contains gneiss inclusions. These fragments are probably of sedimentary origin and where they are frequent the rock could be described as migmatite. There is a constant but irregular change between granite and gneiss inclusions along the core. Smaller pegmatite veins are also found in the cores.

The Stockholm granite is a grey homogeneous granite while the gneiss inclusions are anisotropic with a more or less strong schistosity. In ST1 the schistosity of the gneiss inclusions intersects the core at an angle that varies between 30^{o} and 70^{o}. In ST2 the schistosity down to about 70 m is almost parallel to the core. Below this level the angle

between the schistosity and the core is about 50-75°. The strike of the schistosity in the vicinity of the boreholes is about NW-SE and the dip is 40-70°NE.

With the exception of tectonic zones the bedrock is fresh and unweathered. In and around tectonic zones the grey granite becomes red with clear signs of mineral alteration and weathering.

Well defined tectonic zones in ST1 are mapped at 6.6-7.0 m and 34.4-34.7 m. Red colouring and alteration are found in the intervals 4.5-8.5 m and 32.9-38 m. In the second zone alteration to clay is found. Both zones intersect the borehole at an angle of about 60-70°.

Between 76.6 and 77.2 m a small fracture zone with calcite filling intersects the borehole at an angle of about 30°.

In ST2 well defined tectonic zones are mapped at 6.5-7.5 m and 42.5-44.7 m. Red colouring and alteration are found in the intervals 5.5-8.3 m and 41.6-48.5 m. In the last interval there is also a small zone (48.3-48.5 m) with increased fracturing. In the central part of the interval 42.5-44.7 m the rock is partly altered to clay.

The zone 6.5-7.5 m intersects the borehole at an angle of about 70°. Fractures in the zone 41.6-48.5 m intersect the borehole at an angle of about 50-60°.

Besides the above mentioned zones there is a small tectonic zone (<0.5 m) at 69.5 m and a zone with some alteration and red colour but no increased fracturing at the depth 80.6-82.4 m. The alteration partly follows the schistosity which intersects the borehole at an angle of about 75°.

In both boreholes the fracture frequency apart from the tectonic zones is low. Most of the widely spaced fractures are filled with calcite.

6.2.3 Tunnel mapping

The mapping of the geological conditions in the tunnel in the area of the boreholes shows a dominating grey granite with inclusions of gneiss.

The core mapping gives the impression of a heterogeneous bedrock due to lithological variations in the rock. Several rock contacts are found along the cores. The extension of the different rock types, mapped along the cores, are however unknown. Many of

the inclusions are probably just smaller lenses. The bedrock in the tunnel is found to be similar to the bedrock in the cores. It is however impossible to present a detailed mapping of the tunnel. Thus the dominating rock types are described in the tunnel mapping. These types are grey granite, red granite, and also one section with a mixture of grey and red granite. Gneiss inclusions are found in all three rock types with about the same frequency as in the boreholes.

According to the tunnel mapping fracture frequency is low (Figure 6.1). Calcite is found in many fractures.

East of the boreholes two small tectonic zones cross the tunnel (Figure 6.1). In the first zone at 1/850 there is pronounced crushing and a thin film of clay is also found in most fractures. The bedrock in and around the zone is partly red coloured. Strike and dip of the zone is about N45°E/20-45°W. The width of the zone is about 0.5 m.

The second zone at 1/880 m shows a strong crushing together with an almost complete alteration to clay in the central part of the zone. The bedrock east of the zone consists of red granite. West of and in the zone the bedrock is only partly red-coloured. Strike and dip of the zone is about N10-20°E/15-20°E. The width of the zone in the tunnel is 0.5 m.

6.3 HYDROGEOLOGIC CHARACTERIZATION

6.3.1 Borehole characterization

According to the hydraulic tests performed in the boreholes, the highest transmissivity values in borehole ST1 are found in sections 5-15 m, 29-31 m, 33-35 m, and 77-81 m. Also the interval 45-65 m shows high transmissivity. In borehole ST2 high transmissivities are obtained in sections 5-15 m, 41-45 m, 71-73 m, 77-79 m, and 81-83 m.

The general trend of transmissivity versus depth is somewhat different for the two boreholes. The decrease of transmissivity versus depth is more pronounced in borehole ST1. The deeper part of borehole ST2 (below 65 m) in general has a significantly higher transmissivity than in ST1, particularly in the sections 71-73 m, 77-79 m, and 81-83 m.

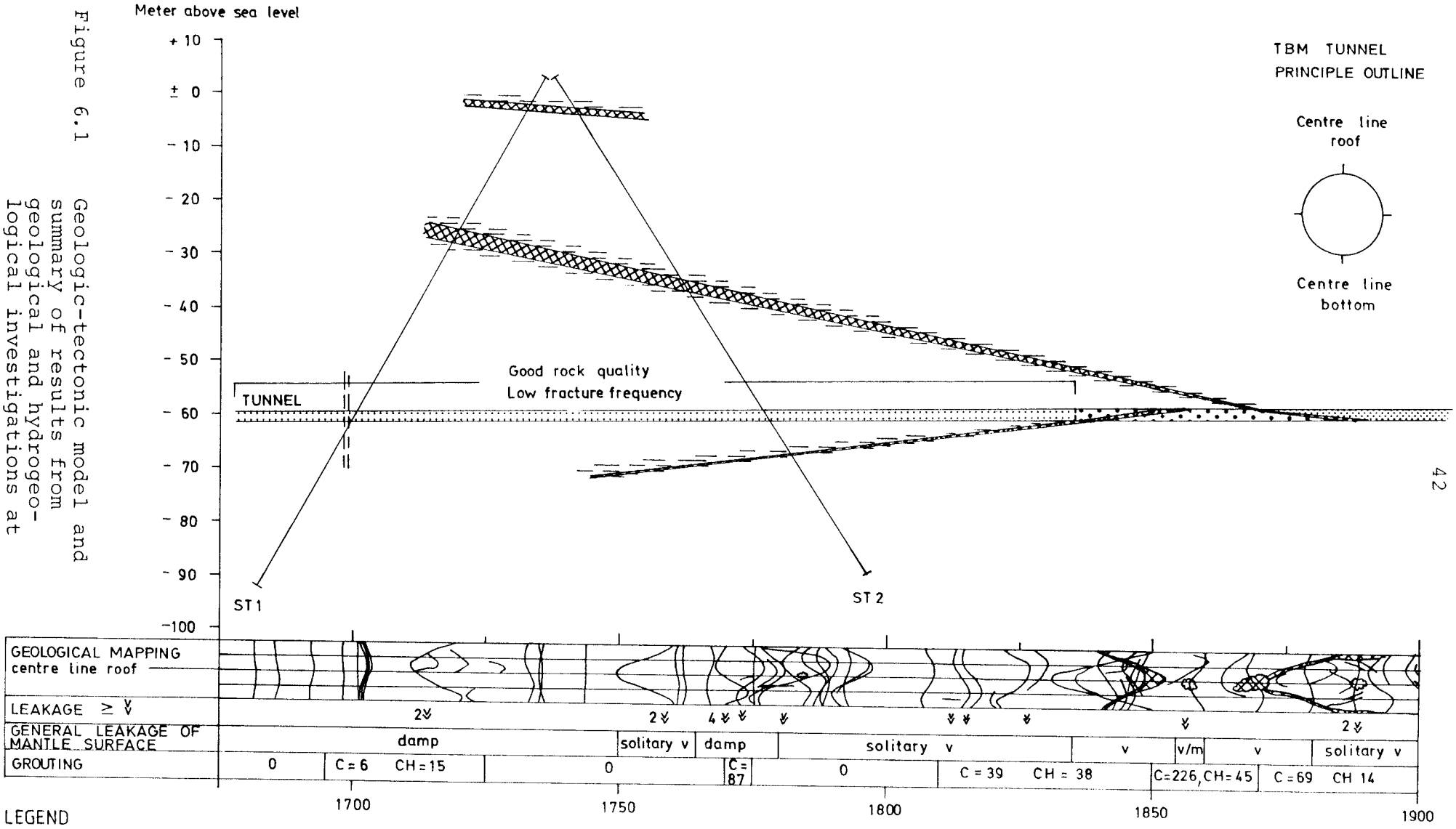

Figure 6.1 Geologic-tectonic model and summary of results from geological and hydrogeological investigations at the Saltsjötunnel site.

The relatively sharp contrast in calculated transmissivities between successive 2 m sections is pronounced in both boreholes. The calculated transmissivities for longer test sections show in general good agreement with the sum of transmissivities for shorter subsections. No information on the interconnectivity between the boreholes can be obtained from the hydraulic tests performed.

6.3.2 Tunnel mapping

Leakage is generally connected to tectonic zones in the bedrock. Relatively large amounts of grout has been injected into the two crush zones which reduces the leakage. In spite of grouting several minor leaks ($\dot{V}$) are noted at the mapping of the tunnel which confirms that these zones are still aquiferous. Because of the grouting it has not been possible to find a simple connection between either degree of crushing and leakage or clay alteration and leakage.

I the bedrock outside the two zones there are some leaks estimated to $\dot{V}$. These leaks are connected to individual aquiferous fractures and horizontal cracks. They also occur in intersection points between horizontal fractures and other fracture directions.

There is also a difference in general water leakage of the mantle surface within and outside crush zones. A general dampness is often noticed outside the crush zones while there is an increasing leakage of the mantle surface within the zones.

6.4 GEOLOGICAL-TECTONIC MODEL

In Figure 6.1 a geological-tectonic model is constructed of information from core mapping and mapping of the tunnel. The greater zones are more or less surrounded by an alteration zone where the bedrock has got a red colour. In the zone crossing the boreholes and the tunnel at 1/880 the central part is altered almost to clay. The zones usually do not follow lithological boundaries.

The zone crossing ST2 and the tunnel at 1/850 does not show the same intensity of crushing in the core as in the tunnel. The signs of alteration are however clearly visible.

The smaller zones in Figure 6.1 lack signs of alteration and are probably quite local with small extension.

The bedrock between the zones generally shows low fracture frequency. Many of the fractures are filled with calcite.

7 COMPARISON OF RADAR PREDICTION WITH TUNNEL RESULTS

The boreholes ST1 and ST2 outline an equilateral triangle and it is within this triangle radar predictions were to be made and compared to data from the drilled tunnel. The tunnel section which is within the triangle extends from tunnel coordinate 1/700 to 1/780. The geological description for this section of the tunnel specifies good rock quality and low fissure frequency. When the location of the boreholes was decided it was hoped that the investigated portion of the rock would contain some significant inhomogeneities which could be mapped by the borehole radar technique and the appearance of these inhomogeneities be observed in the tunnel. Both the radar results and the geological mapping indicate no significant anomalies in the investigated section of the tunnel. Hence, there is general agreement between results but it is difficult to assess the predictive capabilites of the borehole radar method if there are no significant features present. However, some anomalies observed within the investigated triangle can be extrapolated to intersect the tunnel outside of the tunnel section defined by the boreholes.

The revised radar model of the site is described in Section 5.2 and is graphically depicted in Figures 5.9 and 5.10. The results of the hydrogeological mapping in the tunnel and geological mapping on drill cores are shown in Figure 6.1.

The radar attenuation at the Saltsjö site is relatively high with an average value of approximately 0.8 dB/m compared to other sites in Sweden where the borehole radar has been applied. For example average radar attenuation at Stripa was found to be approximately 0.3 dB/m (Olsson, Forslund, Falk, Lundmark, and Sandberg, 1987) and comparable values were obtained at Klipperås (Carlsten, Olsson, Sehlstedt, Stenberg, 1987). The high attenuation at the Saltsjö site resulted in relatively limited radar ranges. The obtained singlehole range was approximately 40 m and the crosshole range was approximately 120 m. From the attenuation tomogram we observe that higher attenuation is generally obtained in the western part (lower tunnel coordinates) of the investigated triangle (Figure 5.9).

High radar attenuation is normally associated with increased fracturing and this was also done in the original radar interpretation of this site. However, both the core mapping data and the tunnel data

indicate relatively low fracture frequencies. The high radar attenuation at this site is most likely caused by the gneissic inclusions in the granite. The gneissic inclusions constitute relatively small inhomogeneities which will scatter the radar waves. Generally an inhomogeneous medium will exhibit higher attenuation than a homogeneous medium even if the constituent parts have low attenuation. This is due to energy loss by multiple scattering. The relatively higher attenuation in the vicinity of ST1 is corroborated by the borehole data (geology and geophysics) which indicate a higher degree of lithological heterogeneity in ST1 than in ST2.

The main feature in the radar data is the one denominated 'A'. This feature exhibits the highest values of attenuation and slowness (inverse velocity) in the tomograms and it is also the most significant feature in the single hole reflection data. The feature was predicted to intersect the tunnel somewhere in the interval 1/860 to 1/910. The uncertainty in the prediction is caused by the small angle between the feature and the extent of the tunnel. This feature is observed in the tunnel as a fracture zone intersecting the tunnel at 1/880. The zone shows strong crushing and almost complete alteration to clay in the central part of the zone. The zone is located in a transition zone between grey granite to the west and red granite to the east. During the drilling of the tunnel relatively large amounts of grout were injected into this zone.

Hence, the major fracture zone at the site was identified by borehole radar and its intersection with the tunnel was correctly predicted. This is also the only zone at the site which have significantly affected the excavation of the tunnel, i.e. required significant grouting efforts.

The radar reflection data indicated the existence of a set of many small reflectors oriented with a strike perpendicular to the tunnel (i.e. NNE) and steeply dipping. This is a common fracture orientation found in the tunnel mapping. There is a concentration of fractures with this orientation in the tunnel interval 1/680 to 1/705 which is considered to correspond to feature 'E' in the radar model. This zone is also included in the geologic-tectonic model.

The revised radar interpretation contains a feature 'K' which would intersect the tunnel at approximately 1/690. At this position in the tunnel there is no increase in fracturing which could be associated with this feature. However, the borehole logs indicate that the feature coincides with a lithological

contact between granite and gneiss. Hence the feature is probably of lithological origin.

The geologic-tectonic model includes a fracture zone intersecting the tunnel at 1/850 dipping gently to the west. This zone intersects borehole ST2 at 81-82 m. This zone is not observed in the radar tomograms but in the reflection data a weak reflector intersecting the borehole at an angle of 50° is observed at the corresponding depth. The degree of crushing observed in the core is smaller compared to what is observed in the tunnel.

8 DISCUSSION AND CONCLUSIONS

The objective of the project described in this report was to investigate the capabilites of the borehole radar technique to predict rock conditions prior to tunnel excavation. The intent was to perform the project as a "blind" test, i.e. a radar interpretation was made without access to any other data in order to see what information could be obtained from radar measurements only. However, in this case the "blind" test was not quite meaningful due to inadequacies of the originally applied tomographic inversion procedure. The first tomograms contained several false anomalies (artifacts) which resulted in a radar interpretation with some erratic features. Hence, it was not considered relevant to compare the original radar model to the data obtained from the tunnel. The comparison is instead made to the revised radar model described in Section 5.2.

The revised radar model is based on the original reflection data and new tomograms which were produced with a recently developed tomographic inversion. The difference between the old tomograms (Figures 5.5 and 5.6) and the new tomograms (Figures 5.9 and 5.10) clearly demonstrate the need for a revised interpretation of the radar data. The main feature, 'A', has retained its position and significance in both radar models. In the revised model smaller weight is given to other features.

The first item of discussion is whether the radar predictions agree with the geology and if the features identified were relevant with respect to excavation of the tunnel. In general there is good agreement between the radar model and the geologic conditions at the site. There is one major feature (A) identified by the radar. This feature is observed as a nearly horizontal structure approximately 25 m above the tunnel with a small dip to the east. The feature was extrapolated to intersect the tunnel somewhere in the interval 1/860-1/910. The actual intersection of the fracture zone was found at 1/880. There is also agreement between a number of smaller features interpreted from the radar data and fracture zones or concentration of fissures observed in the tunnel or boreholes.

With respect to the construction of the tunnel it is clear that only fracture zone 'A' has been of any importance during the excavation (drilling) of the tunnel. At the intersection of this fracture zone with the tunnel significant amounts of grout had to

be applied to reduce the water inflow to the tunnel. It is also clear that the smaller features observed in the radar data has had no effect on the tunnel excavation.

In the original radar interpretation of the Saltsjö tunnel site (and also of other sites investigated at this time) attempts were made to identify as many rock structures as possible. Radar is an investigation method which offers high resolution and this implies that it in many cases is possible to observe very small inhomogeneities in the rock mass. These inhomogeneities are seldom of importance for construction work. Hence, interpretation of radar data for construction purposes should concentrate on the major anomalies apparent in reflection and tomography data.

The second item of discussion is how to apply borehole radar in an efficient manner in connection to tunneling. The setup used for this experiment can not be considered to be cost effective in most cases. Drilling of probing holes from the surface and the performance of measurements in these holes is a relatively costly undertaking. The investigations will yield comparatively detailed information about a relatively short section of the tunnel length (on the order of 100 m). It may well happen, as in this case, that the structural features of importance are not located within the investigated section. However, it should be noted that application of the borehole radar immensely increases the information obtained from a borehole by its ability to record what exists at a distance from the borehole.

Application of radar from the tunnel opens some interesting possibilities. Radar measurements can be made from probe holes ahead of the tunnel front or from the tunnel itself. It is also possible to device measurement configurations where one of the antennas is located in a borehole and the other antenna is located in the tunnel. It should be possible to organize radar measurements in a tunnel in such a way that they can give a continuous prediction of the conditions ahead of the tunnel front at a relatively low cost. This is an area which warrants further research.

This project has demonstrated the capability of the borehole radar technique to predict the existence, location, and orientation of geologic features (e.g. fracture zones) which can be of significance to the cost and safety when excavating a tunnel. However, further development is needed to be able to use the technique cost effectively for continuous prediction ahead of the tunnel front.

9 ACKNOWLEDGEMENT

The authors would like to express their gratitude to STOSEB, the Stockholm Region Energy Company, for their support and assistance in performing the investigations in the tunnel.

This research project is part of a general research programme managed by BeFo, Stockholm, investigating engineering and geological aspects of construction of the Saltsjötunnel in Stockholm by full face boring. This project has been managed and funded by SKB.

10 REFERENCES

Andersson, J.-E., Andersson, P., Carlsten, S., Falk, L., Olsson, O., Stråhle, A., 1987. Combined interpretation of geophysical, geological, hydrological and radar investigations in the boreholes ST1 and ST2 at the Saltsjötunnel. SKB TR 87-14, SKB, Stockholm, Sweden.

Carlsten, S., Falk, L., Olsson, O., 1987. Preliminary interpretation of radar measurements in the boreholes ST1 and ST2 at the Saltsjötunnel. Internal report I 87 333, Swedish Geological Co., Uppsala, Sweden.

Carlsten, S., Olsson, O., Sehlstedt, S., Stenberg, L., 1987. Radar measurements performed at the Klipperås study site. SKB TR 87-01, SKB, Stockholm, Sweden.

Ivansson, S., 1984. Crosshole investigations - Tomography and its application to crosshole seismic measurements. Stripa Project IR 84-08, SKB, Stockholm, Sweden.

Olsson, O., Falk, L., Forslund, O., Lundmark, L., Sandberg, E., 1987. Crosshole investigations - Results from borehole radar investigations. Stripa Project TR 87-11, SKB, Stockholm, Sweden.

Palmqvist, K., Lindström, M., 1988. The Saltsjö TBM tunnel - Hydrogeological mapping and analysis. SKB AR 88-36, SKB, Stockholm, Sweden.

Stålhös, G., 1969. Beskrivning till Stockholmstraktens berggrund (Description to the geological map sheet of Stockholm with surroundings). Swedish Geological Survey, Ser. Ba 24. Uppsala, Sweden. (In Swedish with English summary).

List of SKB reports

Annual Reports

1977–78
TR 121
KBS Technical Reports 1 – 120.
Summaries. Stockholm, May 1979.

1979
TR 79–28
The KBS Annual Report 1979.
KBS Technical Reports 79-01 – 79-27.
Summaries. Stockholm, March 1980.

1980
TR 80–26
The KBS Annual Report 1980.
KBS Technical Reports 80-01 – 80-25.
Summaries. Stockholm, March 1981.

1981
TR 81–17
The KBS Annual Report 1981.
KBS Technical Reports 81-01 – 81-16.
Summaries. Stockholm, April 1982.

1982
TR 82–28
The KBS Annual Report 1982.
KBS Technical Reports 82-01 – 82-27.
Summaries. Stockholm, July 1983.

1983
TR 83–77
The KBS Annual Report 1983.
KBS Technical Reports 83-01 – 83-76
Summaries. Stockholm, June 1984.

1984
TR 85–01
Annual Research and Development Report 1984
Including Summaries of Technical Reports Issued during 1984. (Technical Reports 84-01– 84-19)
Stockholm June 1985.

1985
TR 85-20
Annual Research and Development Report 1985
Including Summaries of Technical Reports Issued during 1985. (Technical Reports 85-01-85-19)
Stockholm May 1986.

1986
TR 86-31
SKB Annual Report 1986
Including Summaries of Technical Reports Issued during 1986
Stockholm, May 1987

1987
TR 87-33
SKB Annual Report 1987
Including Summaries of Technical Reports Issued during 1987
Stockholm, May 1988

1988
TR 88-32
SKB Annual Report 1988
Including Summaries of Technical Reports Issued during 1988
Stockholm, May 1989

Technical Reports

1989
TR 89-01
Near-distance seismological monitoring of the Lansjärv neotectonic fault region Part II: 1988
Rutger Wahlström, Sven-Olof Linder, Conny Holmqvist, Hans-Edy Mårtensson
Seismological Department, Uppsala University, Uppsala
January 1989

TR 89-02
Description of background data in SKB database GEOTAB
Ebbe Eriksson, Stefan Sehlstedt
SGAB, Luleå
February 1989

TR 89-03
Characterization of the morphology, basement rock and tectonics in Sweden
Kennert Röshoff
August 1988

TR 89-04
SKB WP-Cave Project
Radionuclide release from the near-field in a WP-Cave repository
Maria Lindgren, Kristina Skagius
Kemakta Consultants Co, Stockholm
April 1989

TR 89-05
SKB WP-Cave Project
Transport of escaping radionuclides from the WP-Cave repository to the biosphere
Luis Moreno, Sue Arve, Ivars Neretnieks
Royal Institute of Technology, Stockholm
April 1989

TR 89-06
SKB WP-Cave Project
Individual radiation doses from nuclides contained in a WP-Cave repository for spent fuel
Sture Nordlinder, Ulla Bergström
Studsvik Nuclear, Studsvik
April 1989

TR 89-07
SKB WP-Cave Project
Some Notes on Technical Issues
Part 1: Temperature distribution in WP-Cave: when shafts are filled with sand/water mixtures
Stefan Björklund, Lennart Josefson
Division of Solid Mechanics, Chalmers University of Technology, Gothenburg, Sweden
Part 2: Gas and water transport from WP-Cave repository Luis Moreno, Ivars Neretnieks
Department of Chemical Engineering, Royal Institute of Technology, Stockholm, Sweden
Part 3: Transport of escaping nuclides from the WP-Cave repository to the biosphere. Influence of the hydraulic cage
Luis Moreno, Ivars Neretnieks
Department of Chemical Engineering, Royal Institute of Technology, Stockholm, Sweden
August 1989

TR 89-08
SKB WP-Cave Project
Thermally incuded convective motion in groundwater in the near field of the WP-Cave after filling and closure
Polydynamics Limited, Zürich
April 1989

TR 89-09
An evaluation of tracer tests performed at Studsvik
Luis Moreno[1], Ivars Neretnieks[1], Ove Landström[2]
[1] The Royal Institute of Technology, Department of Chemical Engineering, Stockholm
[2] Studsvik Nuclear, Nyköping
March 1989

TR 89-10
Copper produced from powder by HIP to encapsulate nuclear fuel elements
Lars B Ekbom, Sven Bogegård
Swedish National Defence Research Establishment
Materials department, Stockholm
February 1989

TR 89-11
Prediction of hydraulic conductivity and conductive fracture frequency by multivariate analysis of data from the Klipperås study site
Jan-Erik Andersson[1], Lennart Lindqvist[2]
[1] Swedish Geological Co, Uppsala
[2] EMX-system AB, Luleå
February 1988

TR 89-12
Hydraulic interference tests and tracer tests within the Brändan area, Finnsjön study site
The Fracture Zone Project – Phase 3
Jan-Erik Andersson, Lennart Ekman, Erik Gustafsson, Rune Nordqvist, Sven Tirén
Swedish Geological Co, Division of Engineering Geology
June 1988

TR 89-13
Spent fuel
Dissolution and oxidation
An evaluation of literature data
Bernd Grambow
Hanh-Meitner-Institut, Berlin
March 1989

TR 89-14
The SKB spent fuel corrosion program
Status report 1988
Lars O Werme[1], Roy S Forsyth[2]
[1] SKB, Stockholm
[2] Studsvik AB, Nyköping
May 1989

TR 89-15
Comparison between radar data and geophysical, geological and hydrological borehole parameters by multivariate analysis of data
Serje Carlsten, Lennart Lindqvist, Olle Olsson
Swedish Geological Company, Uppsala
March 1989

TR 89-16
Swedish Hard Rock Laboratory – Evaluation of 1988 year pre-investigations and description of the target area, the island of Äspö
Gunnar Gustafsson, Roy Stanfors, Peter Wikberg
June 1989

TR 89-17

Field instrumentation for hydrofracturing stress measurements
Documentation of the 1000 m hydrofracturing unit at Luleå University of Technology

Bjarni Bjarnason, Arne Torikka

August 1989